

1 Responses of estuarine circulation to the morphological evolution in a  
2 convergent, microtidal estuary

3 Rui Zhang<sup>a</sup>, Bo Hong<sup>b</sup>, Lei Zhu<sup>a,c,d</sup>, Wenping Gong<sup>a,c\*</sup>, Heng Zhang<sup>a,c,d</sup>

4 a- School of Marine Sciences, SunYat-sen University, Guangzhou, China, 510275

5 b- School of Civil Engineering and Transportation, South China University of  
6 Technology, Wushan RD., Tianhe District, Guangzhou 510641, China

7 c- Southern Marine Science and Engineering Guangdong Laboratory (Zhuhai), Zhuhai  
8 519000, China

9 d- Pearl River Estuary Marine Ecosystem Research Station, Ministry of Education,  
10 Zhuhai, 519082, China

11  
12 **Abstract:**

13 The Huangmaohai Estuary (HE) is a funnel-shaped microtidal estuary in the west  
14 of the Pearl River Delta (PRD) in southern China. Since China's reform and opening up  
15 in 1978, extensive human activities have occurred and greatly changed the estuary's  
16 topography, and modified its hydrodynamics. In this study, we examined the  
17 morphological evolution by analyzing remote sensing data with ArcGIS tools and  
18 studied the responses of hydrodynamics to the changes in topography from 1977 to  
19 2010 by using the Delft3d model. We took the changes in estuarine circulation during  
20 neap tides in dry seasons as an example. The results show that human reclamation  
21 caused a narrowing of the estuary, and channel dredging deepened the estuary. These  
22 human activities changed both the longitudinal and lateral estuarine circulations. The  
23 longitudinal circulation was observed to increase with the deepening and narrowing of  
24 the estuary. The lateral circulation experienced changes in both the magnitude and  
25 pattern. The momentum balance analysis shows that when the depth and width changed  
26 simultaneously, the longitudinal estuarine circulation was modulated by both the

\* Supported by the National Natural Science Foundation of China under contract Nos 51761135021,  
41506102 and 41890851.

\*\* Corresponding author, E-mail: gongwp@mail.sysu.edu.cn

27 channel deepening and width reduction, in which the friction, pressure gradient force,  
28 and advection terms were altered. The analysis of the longitudinal vortex dynamics  
29 indicates that the changes in the vertical shear of the longitudinal flow, lateral salinity  
30 gradient, and vertical mixing were responsible for the change in the lateral circulation.  
31 The changes in water depth are the dominant factor affecting lateral circulation intensity.  
32 This study has implications for sediment transport and morphological evolution in  
33 estuaries heavily impacted by human interventions.

34

35 **Keywords:** Estuarine circulation, Morphological evolution, Huangmaohai Estuary

36

## 37 **1. Introduction**

38

39 Estuarine circulation, the tidally averaged flow in estuaries including both the  
40 longitudinal and lateral circulations, is the main driving force for the transport of  
41 sediment, pollutants, and other materials, and also one of the primary factors affecting  
42 the ecological environment of estuaries (Kjerfve et al., 1981). Estuarine circulation is  
43 influenced by many factors (Geyer and Maccready, 2014), such as sea-level  
44 fluctuations (Wilson and Filadelfo, 1986), river discharge, tides (Pritchard, 1952), and  
45 winds (Scully et al., 2005; Waterhouse et al., 2013; Geyer and Maccready, 2014; Salles  
46 et al., 2015; Chen et al., 2020a). Topography in an estuary has a significant effect on  
47 the pattern and intensity of the estuarine circulation (Fischer, 1976; Dyer, 1977).  
48 Human activities may change the estuarine topography, leading to changes in the  
49 estuarine circulation and associated material transport. Therefore, a study of the  
50 estuarine circulation and its response to human activities is essential for integrated  
51 management of the development of estuarine resources, and the maintenance of the  
52 estuary's ecological health.

53 Channel deepening by dredging and sand mining is a common practice in the  
54 development and maintenance of navigable channels in estuaries. Generally speaking,  
55 channel deepening can increase the longitudinal estuarine circulation by decreasing the

56 bottom friction and increasing the baroclinic forcing which is proportional to the water  
57 depth (Amin, 1983; Chernetsky et al., 2010; Winterwerp, 2011). On the other hand, the  
58 increase in water depth can also increase the salt intrusion and decrease the along-  
59 channel density gradient, thus reducing the baroclinic forcing. Channel deepening also  
60 affects the estuarine circulation in other ways, such as increasing the Stokes transport  
61 and the associated compensating return flow (Amin, 1983), altering the nonlinear tidal  
62 rectification (Li and O'Donnell, 1997), and tidal asymmetry in mixing between flood  
63 and ebb tides (tidal straining) (Simpson, 1990). Therefore, the effect of channel  
64 deepening is an intricate balance between these reinforcing and/or competing effects.  
65 Chant et al. (2018) demonstrated that a relatively small (15%) increase in water depth  
66 can result in a double exchange flow. They attributed this increase to the increase in  
67 along-channel salinity gradient and/or a reduction in vertical mixing, but they did not  
68 give a clear distinction about how these two effects work together and which is  
69 dominant.

70 Change in estuary width is another aspect of topographic change in estuaries and  
71 is mainly caused by reclamation and utilization of salt marshes, construction of coastal  
72 protection structures along the estuarine banks. Change in estuary width generates a  
73 change in the estuarine convergence, and therefore a change in the estuarine circulation.  
74 Burchard et al. (2014) concluded that an increase in the estuarine convergence results  
75 in an enhancement or reduction of the longitudinal estuarine circulation as increased  
76 estuarine convergence can reduce or even reverse the straining-induced circulation,  
77 though the advection-induced circulation is increased. Changes in estuarine width can  
78 also modify the lateral circulation and feedback to the generation of the longitudinal  
79 estuarine circulation through the change in lateral advection (Lacy et al., 2003; Lerczak  
80 and Rockwell Geyer, 2004; Scully et al., 2009; Burchard et al., 2010; Burchard et al.,  
81 2014). Lerczak and Rockwell Geyer (2004) suggested that lateral effects on the  
82 longitudinal estuarine circulation would be stronger in narrower estuaries given a  
83 constant lateral salinity gradient. Schulz et al. (2015) investigated the impact of the  
84 depth-to-width ratio of the estuarine cross-section on the longitudinal estuarine

85 circulation and found that the longitudinal estuarine circulation exhibits a distinct  
86 maximum in medium-wide channels. They diagnosed the mechanisms for such a  
87 phenomenon and attributed it to the sensitivities of the straining- and advection-induced  
88 circulations on the changes in depth-to-width ratio.

89 As revealed by Lerczak and Geyer (2004) and other researchers (Chen et al.,  
90 2020b), lateral processes play important roles in the generation of the longitudinal  
91 estuarine circulation. In estuaries, the pattern and intensity of lateral circulation are  
92 controlled by three processes (Li et al., 2014): vertical shear of the longitudinal current  
93 affecting the tilting of planetary vorticity, lateral salinity gradient (baroclinicity), and  
94 diffusion. The longitudinal estuarine circulation can affect the lateral circulation  
95 through all the mentioned three factors. Therefore, the interaction between the  
96 longitudinal and lateral processes is fully nonlinear and quite complex. Though these  
97 interactions have been discussed in detail (Scully et al., 2009; Li et al., 2017), several  
98 questions remain open: How does the longitudinal estuarine circulation affect the  
99 intensity and vortex structure of the lateral circulation? Does a decreased/increased  
100 lateral circulation necessarily lead to a weakened/strengthened longitudinal circulation?  
101 These questions become complicated in an estuary where both width and depth vary.  
102 Previous studies showed that the narrowing and deepening of the Yangtze River  
103 Estuary resulted in an enhanced longitudinal estuarine circulation (Zhu, 2018), which  
104 changed from transversely sheared to vertically sheared. The estuarine stratification  
105 was also found to be strengthened, along with an increase in the intensity of lateral  
106 circulation. Zhu et al. (2015) investigated the influences of channel deepening and  
107 widening on the tidal and nontidal circulations of Tampa Bay, USA, and found that the  
108 nontidal circulation was strengthened by these human interventions. However, how  
109 does the estuarine circulation respond to both narrowing and deepening/shallowing of  
110 the estuary? What happens when the narrowing rate is much larger or smaller than the  
111 deepening rate in an estuary? Here the narrowing rate is the ratio of the difference of  
112 cross-section widths between two consecutive years divided by the width in the earlier

113 year. Similarly, the deepening rate is the ratio of the difference of water depth in the  
114 cross-section between the two consecutive years divided by the earlier year's depth.

115 Here we try to address the above questions by studying the changes in the estuarine  
116 circulation from 1977 to 2010 in the Huangmaohai Estuary (HE), a microtidal estuary  
117 in the southwest of the Pearl River Delta (PRD), which experienced different stages of  
118 topographic changes under human activities: narrowing and deepening (1977-1994, and  
119 2003-2010), and narrowing and shallowing (1994-2003). Thus, it provided a good  
120 opportunity to study the effect of human activities induced morphological evolution on  
121 the estuarine circulation.

122 In this study, we used a state-of-the-art three-dimensional baroclinic model (Delft  
123 3d) to simulate the changes in hydrodynamics in the HE in different years and examined  
124 the changes in intensities of the longitudinal and lateral estuarine circulations, followed  
125 by an analysis of the mechanisms for these changes by conducting diagnostic analyses  
126 of the momentum balance. The structure of the rest of the paper is as follows. Section  
127 2 introduces the study area and numeral model. Section 3 presents the results of  
128 morphological evolution and changes in the estuarine circulation. Then, the  
129 mechanisms for the changes in estuarine circulation are investigated using the  
130 momentum and vortex balance equations in Section 4. Finally, the conclusions are  
131 presented in Section 5.

132

## 133 **2. Study area and methodology**

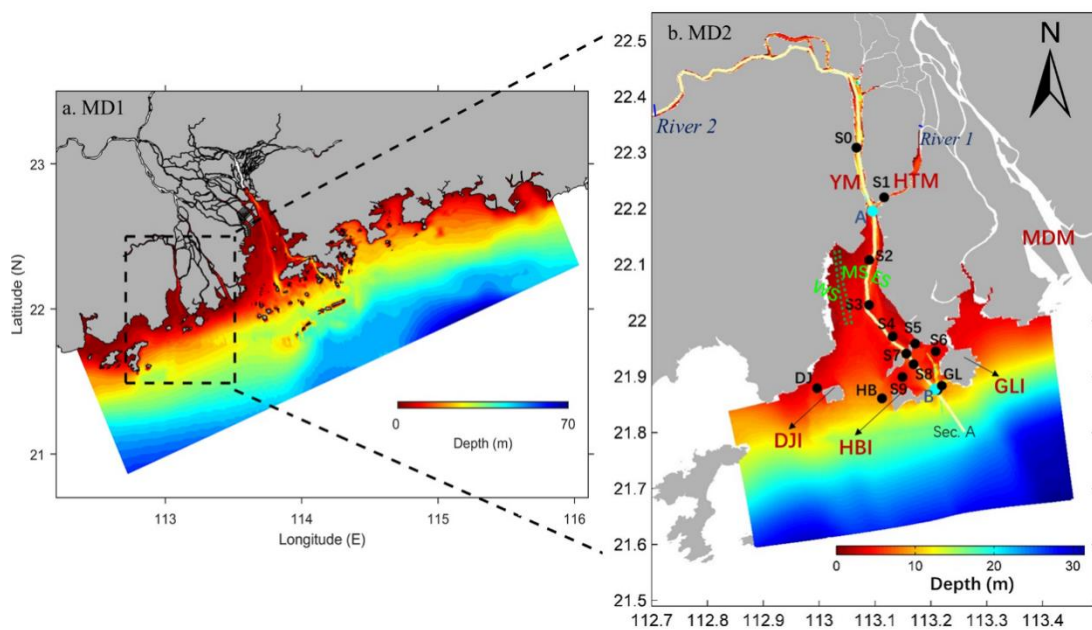
134

### 135 **2.1 Study area**

136

137 The HE is located in the west of the PRD in southern China and exhibits a  
138 distinctly convergent geometry, with a latitude ranging from 21°50' to 22°13' N and  
139 a longitude ranging from 113°00' to 113°51' E (Fig. 1). The estuary is composed of a  
140 bay (Huangmao Bay) and a tidal river. The bay is trumpet-shaped with an area of 409

141 km<sup>2</sup>. It has a complex bathymetry comprising of two channels and three shoals, namely  
 142 the West Channel and East Channel, the West Shoal, Middle Shoal, and East Shoal. In  
 143 recent decades, the West Channel is observed to shrink and almost disappear now (Jia  
 144 et al., 2012). The width of the bay is 30 km at the estuary mouth and decreases to 1.8  
 145 km at the head. The mean water depth of the bay is 4.5 m (Gong et al., 2014). The bay  
 146 is connected to the upstream river catchment by two constrictions (Yamen and  
 147 Hutiaomen Outlets). Several islands, namely Dajin Island, Hebao Island, and Gaolan  
 148 Island, are scattered at the estuary's mouth (shown in Fig. 1b).



149  
 150 Fig. 1. The study area (Huangmaohai estuary) and observation stations. Major topographic  
 151 features and domains of the nested modeling system over (a) the PRD and (b) the HE and its  
 152 adjacent waters. YM = Yamen; HTM = Hutiaomen; MDM = Modaomen; DJI = Dajing Island;  
 153 GLI = Gaolan Island; HBI = Hebao Island. The black dots (S0–S9, DJ, HB, and GL) in the  
 154 MD2 domain are stations of field deployments in March 2010. The solid lines represent the  
 155 along-channel transect (Section A (AB)), which lies in the East Channel. The green dotted lines  
 156 represent the West Channel in 1977. Three shoals are shown in (b): West Shoal (WS), Middle  
 157 Shoal (MS), and East Shoal (ES).

158  
 159 The HE has a subtropical monsoon climate, with the precipitation in the wet season  
 160 (from May to September) being high. Approximately 80% of the river discharge occurs  
 161 during the wet season, with an average discharge of 200.23 m<sup>3</sup>/s. The tides in the HE  
 162 are mixed semidiurnal with dominant semi-diurnal constituents and smaller diurnal

163 constituents. The tidal range is approximately 1.5 m at the mouth and experiences an  
164 initial increase from the mouth towards the head owing to a strong convergence of the  
165 bay width. Further landward in the tidal river beyond the bay head, the tidal range  
166 decreases by the overwhelming bottom friction (Gong et al., 2012). The tidal current  
167 velocity ranges from 0.5 m/s to 1.5 m/s (Huang, 2011), and is higher in deep channels  
168 than on shallow shoals. The tidal currents are generally rectilinear in deep channels but  
169 become more rotary in shallow shoals.

170 Since the 1980s, human activities have been intense in the HE. A hydroelectric  
171 power project upstream of the estuary, channel dredging, sand mining, and construction  
172 of Gaolan Island levees have led to great changes in the HE's topography. Also, the HE  
173 has rich tidal flat resources and endured frequent reclamation activities. From 1965 to  
174 2003, a total of 142.29 km<sup>2</sup> tidal flat was reclaimed, with an average reclamation rate  
175 of 3.74 km<sup>2</sup>/a, and the reclamation rate continuously but gradually increased during that  
176 period. After 2003, the reclamation rate slowed down. In terms of channel dredging,  
177 the Yamen Waterway Project was conducted in 1997 to deepen the channel between  
178 S0 and S3 in Fig. 1b (Luo, 2010). In April 2005, the Yamen Channel regulation project  
179 was implemented to alleviate the serious siltation in the channel, with the channel being  
180 dredged to a depth of about 6 m.

181 In the following, we chose 1977, 1994, 2003, and 2010 as the representative years  
182 to study the typical scenarios of bathymetric changes in the HE.

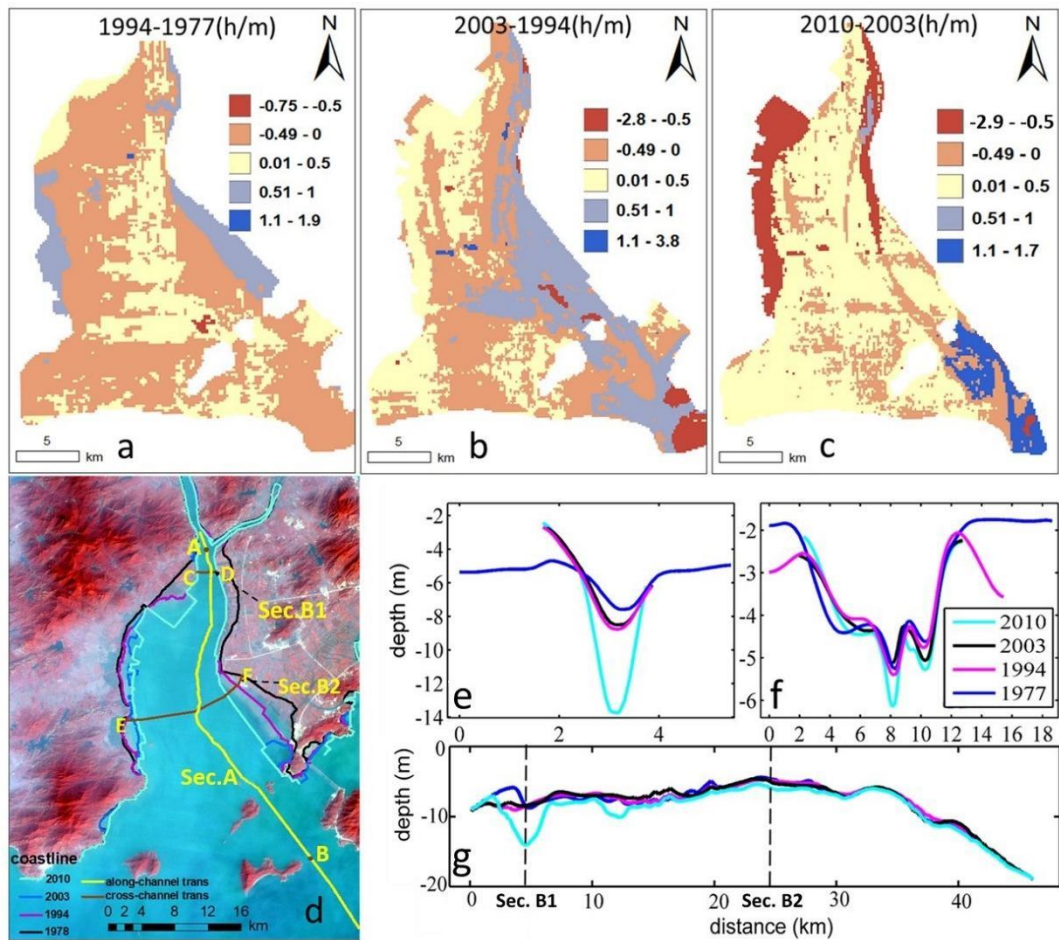
183

## 184 **2.2 Remote sensing and topographic data**

185

186 Remote sensing data were used for coastline extraction and included Landsat  
187 Multi-Spectral Scanner (MSS) data, Landsat Thematic Mapper (TM) data, and Landsat  
188 Operational Land Imager (OLI) data. A total of 66 images (Table 1) were downloaded  
189 from <http://www.gscloud.cn/>. These data were firstly processed by geometric (with  
190 errors less than 0.5 pixels (Ai et al., 2019)) and atmospheric corrections by the ENVI  
191 5.3 software. The topography data inside the HE were derived from nautical charts

192 (1977, 1994, 2003, and 2010), published by the Navigation Safety Guarantee Bureau.  
 193 The filling and excavation toolbox of ArcGIS was used to calculate the difference  
 194 between the volumes in two consecutive periods by superimposing the corresponding  
 195 Digital Elevation Models (DEM). We thus obtained the average siltation rates of the  
 196 study area over different years (Figs. 2a-c).



197  
 198 Fig. 2. (a-c) Water depth difference between two consecutive years ((a)1994-1977; (b)2003-  
 199 1994; (c)2010-2003), where the positive value indicates “deepening” and the negative one  
 200 indicates “siltation”, (d) Shorelines of 1977-2010 and locations of two cross-sections (AB: Sec.  
 201 A; CD: Sec. B1; EF: Sec. B2); (e, f, and g) The bathymetric evolutions at Sections B1, B2, and  
 202 A in 1977, 1994, 2003, and 2010.

203  
 204 Table 1. Data of remote sensing images

Time	Satellite	Image sensor	Resolution/m	Path/Row	Memory space
1973,1978	Landsat3	MSS	78		
1986-2011	Landsat5	TM	30	122/45	142G



2012	Landsat7	ETM	30
2013-2018	Landsat8	OLR	30

205

206 **2.3 Numerical model setting up and validation**

207

208 The numerical model Delft3d, a fully three-dimensional hydrodynamic water quality  
209 model (Lesser et al., 2004), was used to simulate the hydrodynamics in the HE. Its  
210 algorithm can guarantee the conservation of mass, momentum, and energy. The model  
211 grid consisted of a nesting grid system, with the MD1 (parent model, Fig. 1a) covering  
212 the whole PRD, and the MD2 (child model) covering the HE. For the MD2 model, a  
213 curvilinear orthogonal grid of 269\*620 was established, with the horizontal resolution  
214 ranging from 85 m in the channel to 324 m at the ocean boundary. Vertically, the grid  
215 was discretized into 10 layers of  $\sigma$  coordinate. The model system used here is the same  
216 as the one in Chen et al. (2020a). The MD1, based on a 1-D (for the river network) and  
217 3-D coupled model, covered the whole PRD and the coastal region with a horizontal  
218 resolution of 2 km near the open boundary and 500 m inside the PRE (Fig. 1a). The  
219 Open sea boundaries for the MD1 comprised hourly tidal elevations and depth-averaged  
220 tidal currents derived from nine tidal constituents (M2, S2, N2, K2, K1, O1, P1, Q1,  
221 and M4) taken from the global tidal circulation model (TPXO 8,  
222 [http://volkov.oce.orst.edu/tides/tpxo8\\_atlas.html](http://volkov.oce.orst.edu/tides/tpxo8_atlas.html)) with a resolution of  $1/30^\circ$  and daily  
223 water elevation, 3-D temperature, salinity (a constant salinity of 34 psu at the open  
224 ocean boundary) and velocity data from the Hybrid Coordinate Ocean Model  
225 (<https://hycom.org>) with a resolution of  $1/12^\circ$  (Chen et al., 2020a). Thus the sources of  
226 water level variation and currents at the offshore boundary in MD1 are: 1) tides; 2) non-  
227 tidal components by external forcings, such as winds, air pressure, water temperature,  
228 and large-scale circulation in the South China Sea. The results from the MD1 were  
229 interpolated to provide ocean boundary conditions for the MD2 model, and there were  
230 no “wind and wave effects” in the MD2.

231 As mentioned above, the hydrodynamics in the HE experiences distinct seasonal  
 232 variation. The estuarine circulation during the wet season has been extensively studied  
 233 before (Chen et al., 2020a; Chen et al., 2020b). Here we choose the dry season to  
 234 investigate the changes in the estuarine circulation caused by topographic changes in  
 235 different years. We conducted a series of numerical experiments using the bathymetry  
 236 data in 1977, 1994, 2003, and 2010. The simulation time was chosen to be from 00:00  
 237 on March 1 to 23:00 on March 31 in the dry season, when observation data were  
 238 available in 2010. Field measurements were carried out at 14 mooring stations on  
 239 March 17th 17:00 to 18th 22:00, 2010. The measured variables included vertical  
 240 profiles of current, temperature, and salinity. In all the four scenarios, two upstream  
 241 boundaries were specified (Fig. 1b): at River 2 by specifying real-time water level data  
 242 from the MD1 model from 00:00 on March 1, 2010, to 23:00 on March 31, 2010, with  
 243 a time interval of 1 hour; At River 1 by specifying a constant river discharge of  $100 \text{ ms}^{-2}$ .  
 244 The choice of this constant value was based on previous simulation experiences  
 245 (Chen et al., 2020a; Chen et al., 2020b). The salinities at the river inflow boundaries  
 246 were set to be 0 psu. The only changing condition of the four scenarios was the  
 247 topography (Table 2), so the effect of topographic change can be distinguished. The  
 248 measured data from 14 stations in 2010 were used to validate the model.

249

250 Table 2. Coastline, bathymetries, salinity, flow, and tidal boundary in the four model scenarios.

Scenario	Coastline	Bathymetrie s	The salinity of the open sea	Flow	Tidal boundary
1977/03	1977	1977	2010/03	2010/03	2010/03
1994/03	1994	1994	2010/03	2010/03	2010/03
2003/03	2003	2003	2010/03	2010/03	2010/03
2010/03	2010	2010	2010/03	2010/03	2010/03

251

252 In this study, the Willmott skill score (SK) was used to evaluate whether the model  
 253 result is consistent with the observed data (Willmott, 1981). The SK is defined as:

$$254 \quad SK = 1 - \frac{\sum_{i=1}^n (O_i - M_i)^2}{\sum_{i=1}^n [ |M_i - \bar{O}| + |O_i - \bar{O}| ]^2} , \quad (1)$$

255 where  $n$  is the number of the observed data,  $M$  and  $O$  are model simulation results  
 256 and observations, respectively, and  $\bar{o}$  is the average value of the observation data. SK  
 257 is used to measure the consistency between the model results and the observations, with  
 258 a value between 0 and 1. The larger the value is, the more consistent the simulation  
 259 results are with the observed data.

260 Firstly, the water level of the MD2 model was validated. The SKs of the four  
 261 observed stations are all above 0.86, indicating that the water level simulation is  
 262 reasonable. Secondly, the modeled current directions showed good performance except  
 263 for the surface layer at Stations DJ and S0, almost all the SKs are greater than 0.7 (Table  
 264 3). The simulation of the current speed is worse than that of the current direction, but  
 265 the SKs at most stations are above 0.6, showing a good performance. Lastly, the trends  
 266 of observed and simulated salinities are consistent, and almost all the SKs of salinity  
 267 validation are above 0.5, especially in S1-S3, showing a good performance of the  
 268 salinity simulation.

269 Table 3. Skill scores by comparison of modeled results with observations.

Stations	Current direction			Current speed			Salinity		
	Sur	Mid	Bot	Sur	Mid	Bot	Sur	Mid	Bot
S0	0.18	0.96	0.96	0.77	0.88	0.86	0.32	0.35	0.35
S1	0.94	0.99	0.99	0.65	0.66	0.61	0.94	0.94	0.90
S2	0.78	0.79	0.71	0.83	0.84	0.84	0.84	0.85	0.85
S3	0.87	0.98	0.95	0.34	0.38	0.39	0.92	0.79	0.77
S4	0.84	0.94	0.94	0.53	0.55	0.53	0.77	0.64	0.54
S5	0.86	0.92	0.93	0.66	0.71	0.72	0.37	0.25	0.26
S6	0.79	0.90	0.88	0.68	0.75	0.74	0.15	0.20	0.25
S7	0.82	0.85	0.96	0.74	0.79	0.83	0.86	0.66	0.56
S8	0.84	0.89	0.89	0.59	0.62	0.66	0.82	0.77	0.72
S9	0.80	0.74	0.77	0.54	0.46	0.41	0.59	0.50	0.52
DJ	0.61	0.77	0.77	0.38	0.47	0.51	0.66	0.47	0.37
GL	0.89	0.91	0.93	0.50	0.51	0.49	0.37	0.43	0.41
HB	0.71	0.89	0.89	0.60	0.56	0.56	0.57	0.54	0.53

270  
 271 As a whole, the simulation of surface currents is worse than that in other layers,  
 272 since winds and waves were not included in our MD2 model simulations, in which the  
 273 surface flow is more susceptible to these forcings. The specified river flow at River 2

274 was constant, which may deviate from the real-time data (not available), leading to a  
275 poor salinity reproduction at upstream stations. In short, the water level and current are  
276 well-validated. The simulation of salinity is generally good, except for some deviations  
277 at upstream stations. It shows that the model can reasonably simulate the hydrodynamic  
278 processes in the area, and can be used for the following hydrodynamics study in the HE.

279

### 280 **3. Results**

281

#### 282 **3.1 Morphological evolution**

283

284 Morphological changes between 1977, 1994, 2003, and 2010 are shown in Figs.  
285 2a-c. Figure 2a shows that most areas in the HE experienced siltation from 1977 to  
286 1994, but the East Channel was deepened by about 0-0.5 m. In the middle of the bay,  
287 the nearshore areas were under erosion, and the erosion thickness at the eastern shore  
288 was twice that at the western shore. In other areas, the siltation thickness was between  
289 0 and 0.5 m. From 1994 to 2003, erosion occurred in the West Shoal, East Channel,  
290 East Shoal, and Middle Shoal. Siltation of 0.01-0.5 m happened in the rest of the area,  
291 which accounted for most of the HE, so the HE became shallower in 2003. In 2003,  
292 siltation in the East Channel was serious and the water depth there became only 2m (Li,  
293 2019). From 2003 to 2010, the West Shoal became significantly shallower with a  
294 siltation thickness of about 0.5-1m. The East Shoal almost disappeared, and its relict  
295 area endured siltation of 1.1-1.7 m, which was mainly due to the construction of coastal  
296 protection works. Strong erosion occurred in other areas, especially in the upper bay  
297 with a deepening of more than 4m, and the overall water depth of the HE became greater  
298 in 2010.

299 Overall, the water depth of the HE changed considerably from 1977 to 2010. It  
300 first experienced erosion, then underwent siltation, and followed by erosion again.

301 Figure 2d shows the changes of coastlines for the four representative years. To  
302 calculate the rate of geometry convergence, the DSAS tool (Version 5.0) in Arcmap  
303 10.3 was used to calculate the end-point rates for cross-shore transects. A more detailed  
304 procedure is in Zhang et al. (2019). We chose one longitudinal section along the channel  
305 in the estuary and two cross-sections (in Fig. 2d) along the channel for analysis. The  
306 longitudinal section (Sec. A) extends from the bay head (point A in Fig. 1b) to the  
307 estuary mouth (point B in Fig. 1b), spanning a distance of 50 km. Sec. B1 is located at  
308 about 4 km downstream from the bayhead, where the water depth changes sharply in  
309 the lateral (or longitudinal) direction (see Fig. 2e). Sec. B2 is approximately 24km  
310 downstream from the bayhead and near the null point in the middle of the estuary (see  
311 Fig. 2f), and the width of the estuary varied dramatically here (see Fig. 2e). At Sec. A,  
312 the water depth near the point of Sec. B1 endured a great change in 2010 due to channel  
313 dredging (Fig. 2g). In other periods, the water depth along its course endured gradual  
314 deepening. At Sec. B1, the bathymetric change is featured by an increase in water depth  
315 and negligible change in width over time. At Sec. B2, both the water depth and width  
316 experienced changes from 1977 to 2010, with the depth increased and width decreased  
317 (Fig. 2f). The above three sections clearly depict the topographic changes of the estuary  
318 in different years.

319

### 320 **3.2 Changes in the vertically averaged flow and salinity**

321

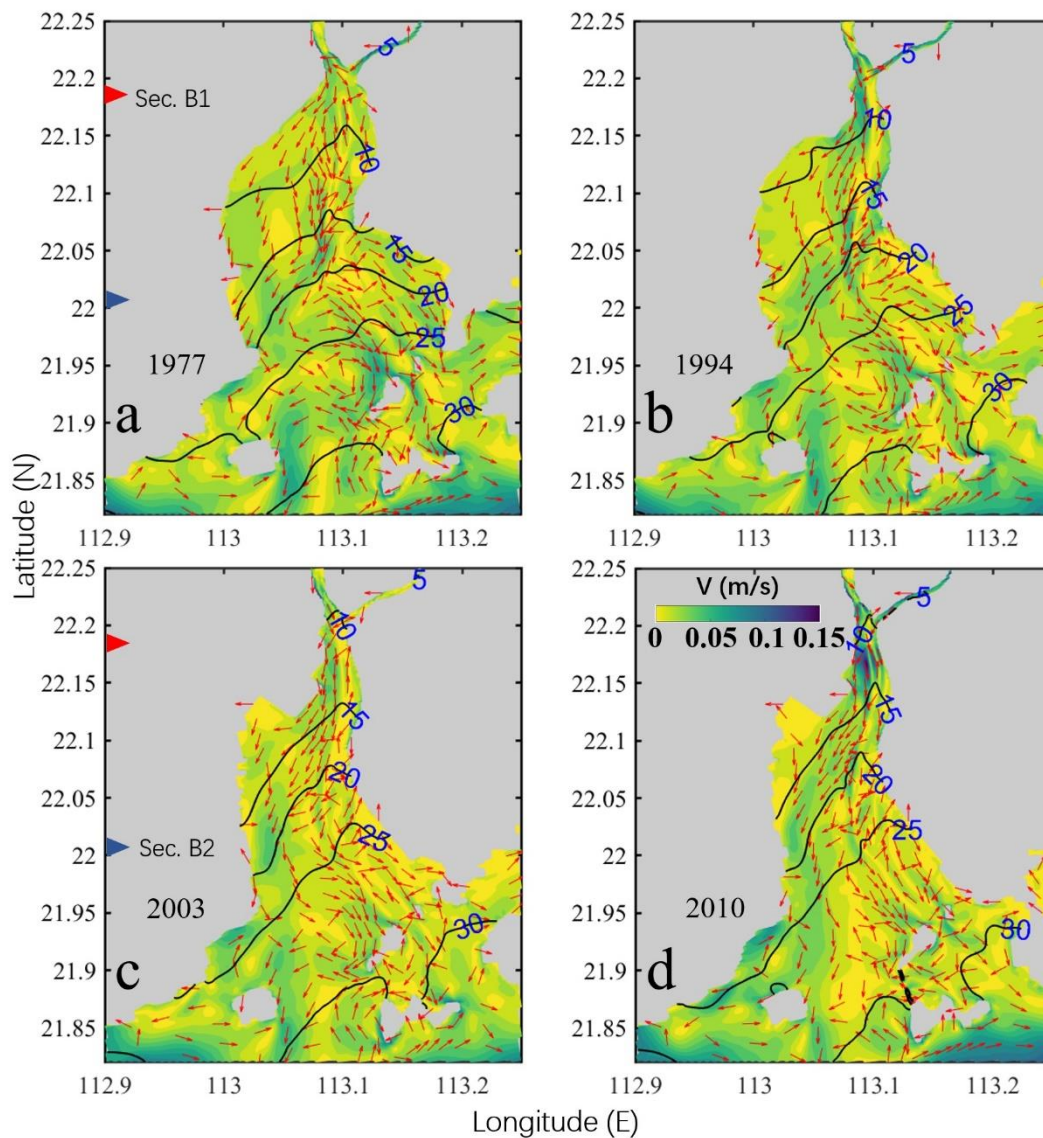
322 Here we present the changes in the tidally and vertically averaged flow and salinity  
323 during neap tides in Fig. 3. In 1977 (Fig. 3a), the current speed was generally small,  
324 except at the inter-island sections and in the channel. The vertically averaged flow was  
325 seaward in the upper bay and the right part of the lower bay (looking landward). It  
326 became landward at the left part of the lower bay. In 1994 (Fig. 3b), the current speed  
327 was increased in the channel, particularly near Sec.B1. The overall flow pattern was  
328 almost similar to that in 1977. In 2003 (Fig. 3c), the flow pattern still kept unchanged  
329 when compared to that in previous years. The current speed was decreased relative to

330 that in 1994. In 2010 (Fig. 3d), the seaward flow became more dominant in the upper  
331 bay, and more biased southwestward. The seaward flow in the channel was greater than  
332 in 2003. The 10 psu isohaline kept moving upstream over time, and reached beyond the  
333 bayhead and entered into the tidal river of the estuary in 2010.

334 Overall, we observed that the tidally and vertically averaged flow during neap tides  
335 experienced an increase-decrease-increase by the topographic changes, whereas the  
336 saltwater consistently intruded more landward.

337 As a supplement, we present the horizontal distributions of tidally averaged  
338 surface and bottom circulation and salinity during neap tides for different years in the  
339 appendix (Figs. A. 1 and 2). Over the study period, the enhancement of salt intrusion  
340 was stronger for the bottom layer and weaker for the surface layer, whereas the increase  
341 in residual flow was stronger in the surface layer and weaker in the bottom layer.

342 For the hydrodynamic characteristics of the HE during the flood and ebb tides,  
343 Chen et al., (2020a) have investigated the intratidal dynamic processes in detail.



344

345 Fig. 3. Patterns of the tidally and vertically averaged circulation during neap tide (from March  
 346 10th 00:00 to 11st 00:00 (25h)) in 1977(a1), 1994(a2), 2003(a3), and 2004(a4). The magnitude  
 347 of the current is represented by the color shading, while the current direction is shown by the  
 348 arrows. The salinity is depicted by the contour lines. The red and blue triangles depict the  
 349 positions of two cross-sections (Sec.B1 and Sec.B2).

350

### 351 3.3 Changes in the estuarine circulation

352

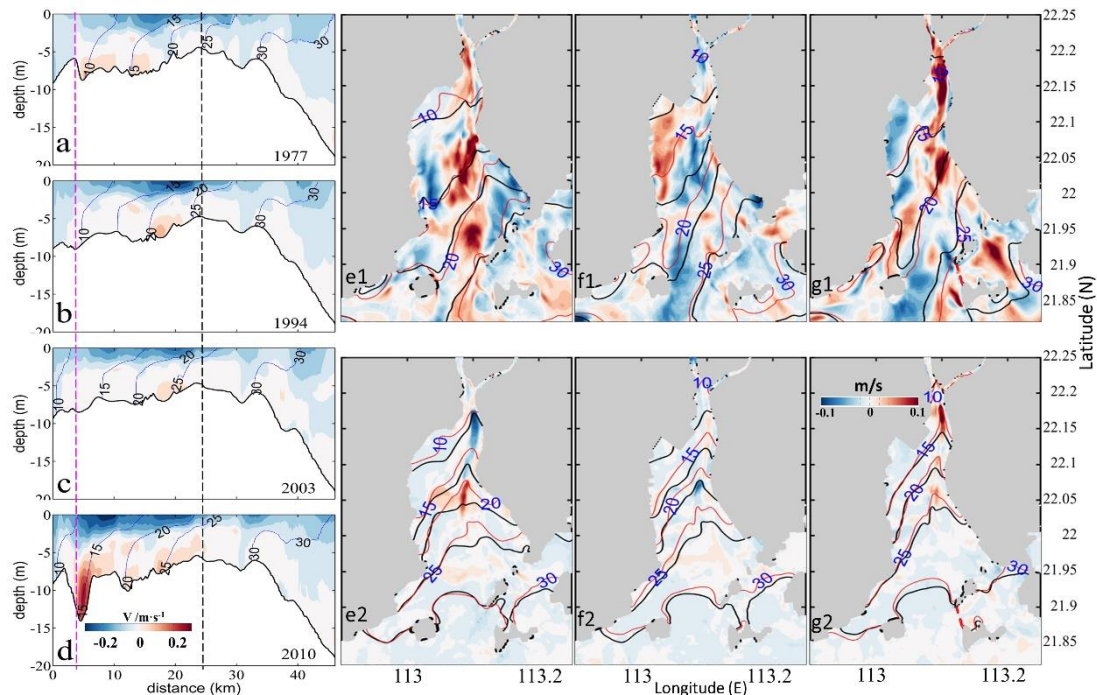
353 Figures 4 a-d show that the upper part of the estuary (upstream of the null point)  
 354 was highly stratified, and the lower part of the estuary (downstream of the null point)  
 355 was well mixed. The classical exchange flow structure was more distinct upstream of

356 the null point. Over time, the surface seaward flow became stronger and more  
357 concentrated with the narrowing of the estuary, particularly in 2010. It extended more  
358 downstream to near the estuary mouth with the narrowing of the estuary, as evidenced  
359 by the extent of the seaward flow of 0.2 m/s. Concomitantly, the bottom landward flow  
360 was strengthened and concentrated with the increase in depth. It should be noted that  
361 the greatly enhanced estuarine circulation between 3 to 8 km in 2010 (Fig. 4d) could be  
362 induced by the intratidal fluctuation of the halocline in response to the large topography  
363 change there (Geyer and Nepf, 1996; Chen et al., 2012; Wang et al., 2015).

364 We also present the changes in the surface and bottom current horizontally. Figs.  
365 4e1-g1 show that when the estuary deepened (1977-1994 and 2003-2010), the surface  
366 current velocity increased in the channel, and when the estuary shoaled (1994-2003),  
367 the surface current velocity in the channel decreased. The changes in the bottom current  
368 showed a similar trend (Figs. 4e2-g2), except at the upper part of the channel from 1977  
369 to 1994, in which the width was considerably decreased.

370 Along with the change in the longitudinal estuarine circulation, the salt intrusion  
371 at Sec. A did not change significantly from 1977 to 1994, but increased from 2003 on,  
372 particularly in 2010, when the isohaline of 15 psu reached Sec.B1, whose salinities  
373 were less than 12 psu in previous years (Figs. 4a-d). The salt intrusions at the surface  
374 and bottom gradually increased with the estuary narrowing (Figs. 4e1-g2).





375

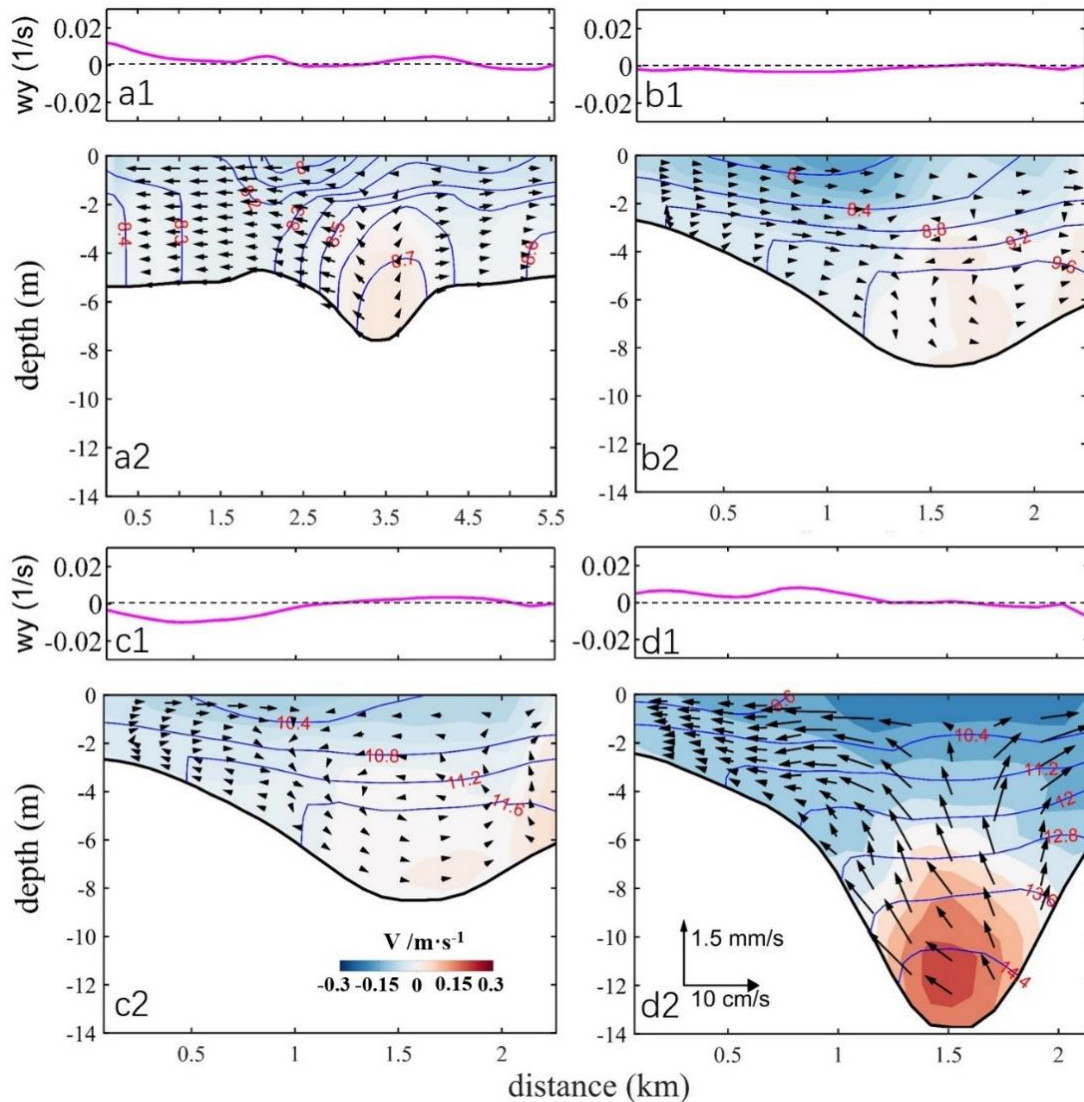
376 Fig. 4. The patterns of the estuarine circulation during the neap tide (from March 10th 00:00 to  
 377 11st 00:00 (25h)) in March 1977(a), 1994(b), 2003(c), and 2010(d). The thin lines are the  
 378 isolines of salinity in a-d. The pink and black dotted lines represent the locations of Secs. B1  
 379 and B2, respectively. The starting point of the X-axis is Point A in Fig. 1b. Surface tidally-  
 380 averaged current differences from 1977 to 1994(e1), from 1994 to 2003(f1), and from 2003 to  
 381 2010(g1); Bottom tidally-averaged current differences from 1977 to 1994(e2), from 1994 to  
 382 2003(f2), and from 2003 to 2010(g2). The red and black lines represent the isolines of salinity  
 383 in the later year and the earlier year.

384

385 To analyze the changes of lateral circulation in the estuary, we show the structure  
 386 and intensity of the lateral circulation at the two cross-sections (Figs. 5 and 6).

387 At Sec. B1 (Fig. 5), with the increase of water depth, the salinity difference  
 388 between the surface and bottom increased, along with an increase in the bottom salinity.  
 389 For the lateral circulation, there was no distinct gyre structure in 1977. In 1994, the  
 390 lateral flow was dominated by an eastward flow. In 2003, a clockwise vortex was  
 391 developed over the West Shoal (0.5-1 km). Meanwhile, an anticlockwise circulation  
 392 with smaller vortex intensity was developed in the region of 1-2km from the western  
 393 shore. Another clockwise circulation was developed over the East Shoal. When the  
 394 estuary became deepened in 2010, the distribution of the lateral circulation was similar

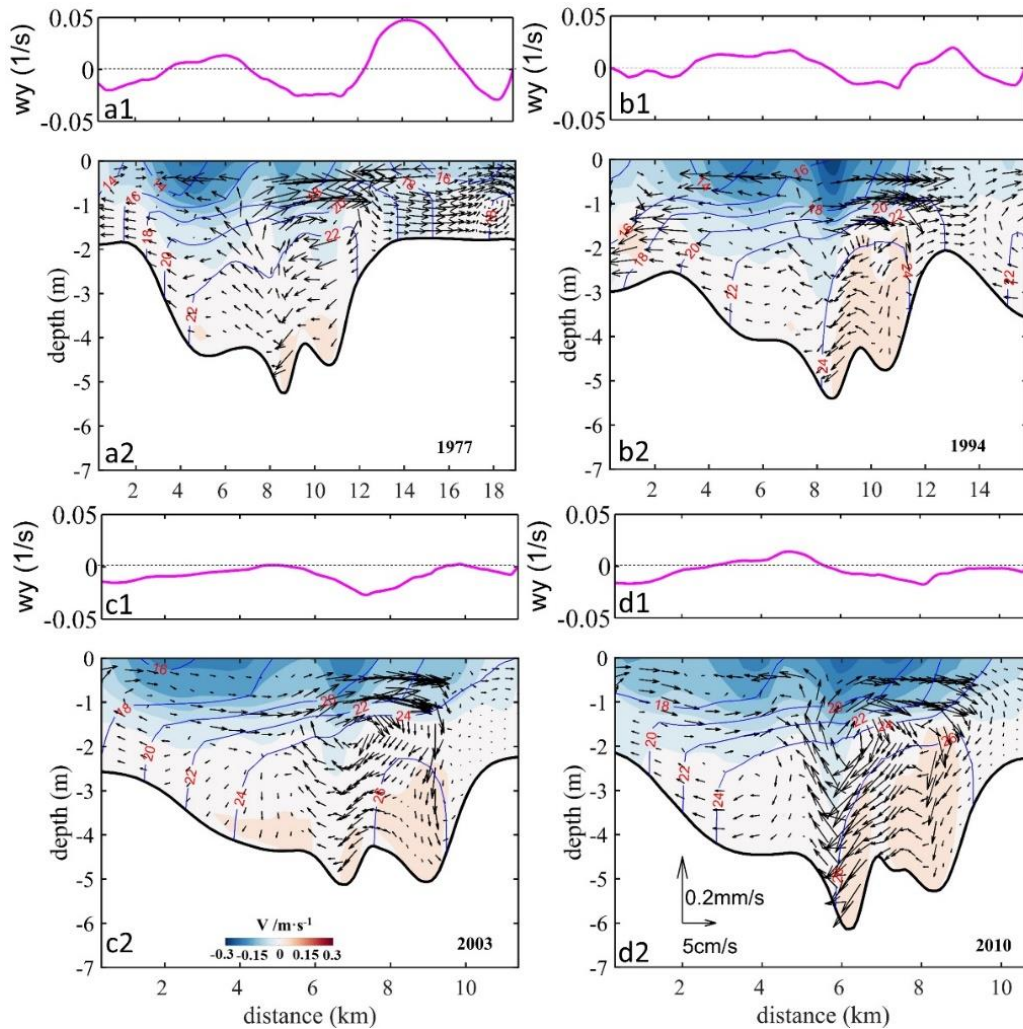
395 to that in 1977, but the vortex intensity increased significantly to about 2-4 times that  
 396 of 1977.



397  
 398 Fig. 5. The tidally-averaged (from March 10th 00:00 to 11st 00:00 (25h)) lateral circulation and  
 399 isohalines (blue lines) at Sec. B1 in 1977(a2), 1994(b2), 2003(c2), and 2010(d2). The starting  
 400 point of the X-axis is Point C in Fig. 2d.  $w_y$  is the longitudinal vorticity at Sec. B1 in 1977(a1),  
 401 1994(a2), 2003(a3), and 2010(a4). The arrows indicate the magnitude of lateral flow and  
 402 vertical flow per unit length: 10 cm/s and 1.5 mm/s, respectively.  
 403

404 Figure 6 shows the changes in lateral circulation at Sec. B2. With the decrease of  
 405 estuary width, the salinity increased in the cross-section over the years. There  
 406 developed a clockwise circulation at the right of the deep channel in 1977 and 1994.  
 407 This clockwise vortex was seen to move westward from 2003 on. The spatial extent of  
 408 the clockwise circulation in the deep channel increased significantly over time.

409 Clockwise vortices developed over the East Shore from 1977 to 2010, but their intensity  
 410 became weaker since 2003. In 1977 and 1994, the distance between the deep channel  
 411 and the East Shore was greater than 2 km which was sufficient for accommodating  
 412 clockwise vortices. From 2003 on, the accommodation space at the East Shore became  
 413 limited and restricted the full development of the clockwise vortex. Over the West  
 414 Shoal, the lateral circulation pattern showed an anticlockwise circulation in 1977 and  
 415 1994. However, since 2003, the lateral circulation over the West Shoal began to develop  
 416 a two-cell pattern, with an anticlockwise gyre at the surface and a clockwise one near  
 417 the bottom. The clockwise cell developed well in 2010.



418  
 419 Fig. 6. The tidally-averaged (from March 10th 00:00 to 11st 00:00 (25h)) lateral circulation and  
 420 isohalines (blue lines) at Sec.B2 in 1977(a2), 1994(b2), 2003(c2), and 2010(d2). The starting  
 421 point of the X-axis is Point E in Fig. 2d.  $w_y$  is the longitudinal vorticity at Sec. B2 in 1977(a1),  
 422 1994(a2), 2003(a3), and 2010(a4). The arrows indicate the magnitude of lateral flow and  
 423 vertical flow per unit length: 5 cm/s and 0.2 mm/s, respectively.

424 As a whole, over the study period, the longitudinal estuarine circulation continued  
425 to increase, whereas the lateral circulation experienced varying changes at different  
426 cross-sections. At the upstream cross-section (B1), when the estuary narrowed, the  
427 original pattern of two-cell vortices with opposite polarity was disrupted. However, it  
428 was amplified in 2010 when the water depth was increased. At the cross-section in the  
429 middle of the estuary (B2), a similar two-cell pattern was developed. However, in 2003  
430 and 2010, the single cell at the West Shoal was split into two cells: an anticlockwise  
431 cell at the surface and a clockwise cell at the lower part.

432

### 433 **3.4 Relationship between the changes in the intensity of estuarine circulation and** 434 **the changes in topography**

435

436 To further quantitatively identify the influence of topographic changes on the  
437 estuarine circulation, we calculated the changes in the intensity of estuarine circulations  
438 in the longitudinal and lateral directions. The magnitude of estuarine circulation in the  
439 longitudinal section was used to represent the intensity of the longitudinal estuarine  
440 circulation (Chen and Sanford, 2009). The method was to subtract the subtidal  
441 longitudinal velocity of the bottom layer from that on the surface layer. The magnitude  
442 of the vorticity in the cross-sections was used to represent the intensity of the lateral  
443 circulation (Becherer et al. 2015), and is expressed as:

$$444 \quad w_y = \partial w / \partial x - \partial u / \partial z \quad (2)$$

445 where,  $w_y$  is the longitudinal vorticity in the cross-sections.  $w$  and  $u$  are the  
446 currents in the vertical and lateral directions, respectively.  $\partial w / \partial x$  is small and can be  
447 ignored, therefore, formula (2) can be simplified as:

$$448 \quad w_y = -\partial u / \partial z \quad (3)$$

449 when  $w_y$  is positive, the lateral circulation is an anticlockwise vortex, conversely,  
450 when  $w_y$  is negative, the lateral circulation is a clockwise vortex.

451 The results of the averaged intensity of estuarine circulation along Sec. A and the  
452 averaged intensity of vorticity at the cross-sections are listed in Table 4.

453 Table 4. The changes of width and depth (the maximum depth), area (cross-section area), w-to-  
 454 d, narrowing rate, deepening rate, and the intensity of circulations (w-to-d: width-to-depth ratio;  
 455 narrowing rate: the ratio of the difference of cross-section widths between two years divided  
 456 by the width in the earlier year; deepening rate: the ratio of the difference of water depth in the  
 457 cross-section between the corresponding two years divided by the earlier depth. The positive  
 458 narrowing rate indicates that the estuary is narrowed; the positive deepening rate indicates that  
 459 the estuary is deepened.)  
 460

		time	1977/03	1994/03	2003/03	2010/03
Sec.B1	width (km)		5.56	2.25	2.26	2.14
	depth (m)		7.58	8.76	8.50	13.73
	w-to-d		734	257	266	156
	area (km <sup>2</sup> )		0.0468	0.0213	0.0207	0.0256
	narrowing rate		\	59.50%	-0.44%	5.30%
	deepening rate		\	15.58%	-2.95%	61.47%
	Sec.B2	width (km)		18.97	15.77	11.40
depth (m)			5.25	5.40	5.12	6.13
w-to-d			3610	2920	2230	1760
area (km <sup>2</sup> )			0.0849	0.303	0.0647	0.0646
narrowing rate			\	16.87%	27.71%	5.61%
deepening rate			\	2.86%	-5.19%	19.73%
circulation intensity		longitudinal	Sec. A	0.0274	0.0428	0.0483
	lateral	Sec. B1	0.0111	0.0146	0.0130	0.0278
		Sec. B2	0.0493	0.0460	0.0465	0.0425

461

462 Table 4 indicates that the longitudinal estuarine circulation intensity increased with  
 463 the estuary narrowing, and was largest (0.0594 m/s) in 2010.

464 The lateral circulation intensity varied in different cross-sections. For Sec.B1, it  
 465 increased gradually when the estuary deepened (from 1994 to 2010). When the  
 466 deepening rate reached the maximum (61.47%) in 2010, the lateral circulation intensity  
 467 reached the maximum as well. The intensity of lateral circulation increased when the  
 468 estuary deepened and narrowed (from 1977 to 1994, and from 2003 to 2010), but it  
 469 decreased when the estuary shallowed and narrowed (from 1994 to 2003). For Sec.B2,  
 470 the intensity of lateral circulation decreased when the estuary deepened and narrowed  
 471 (from 1977 to 1994, and from 2003 to 2010). However, this trend was altered when the  
 472 estuary entered into the “narrowing and shallowing period”, with the deepening rate

473 being -5.19%. It indicates that changes in water depth were the dominant factors  
 474 affecting the lateral circulation intensity.

475 In general, the relationship between the longitudinal estuarine circulation intensity  
 476 and the estuary width showed a monotonic decrease, while that between the  
 477 longitudinal estuarine circulation intensity and the water depth is a monotonic increase,  
 478 but the lateral circulation intensity seemed to have no simple linear relationship with  
 479 the topographic change.

480

## 481 **4. Discussion**

482

### 483 **4.1 Contribution of momentum terms to the variation of the longitudinal** 484 **estuarine circulation**

485

486 To explain the change in the longitudinal estuarine circulation intensity, we  
 487 conducted a diagnostic study by examining the changes in terms of the momentum  
 488 balance equations. We calculated each term of the momentum equation in the  
 489 longitudinal direction in the tidally averaged timescale:

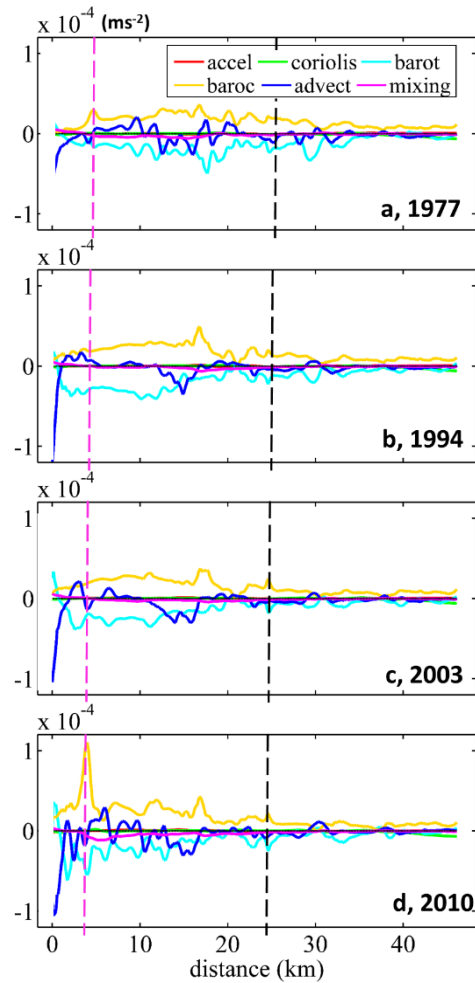
$$490 \quad \frac{\partial v}{\partial t} = \underbrace{fu}_{\text{coriolis}} - \underbrace{g \frac{\partial \eta}{\partial y}}_{\text{barotropic pressure}} - \underbrace{\frac{gz}{\rho_0} \frac{\partial \rho}{\partial y}}_{\text{baroclinic pressure}} - \underbrace{\left( u \frac{\partial v}{\partial x} + v \frac{\partial v}{\partial y} + w \frac{\partial v}{\partial z} \right)}_{\text{advection}} + \underbrace{\frac{\partial}{\partial z} \left( A_v \frac{\partial v}{\partial z} \right)}_{\text{vertical friction}}, \quad (4)$$

491 By comparing the changes in each term and linking them with the characteristics  
 492 of morphological evolution, we explain the response of the longitudinal estuarine  
 493 circulation to bathymetric change in the perspective of momentum balance. Though the  
 494 change in an individual momentum term in Eq. 4 can not represent the change in the  
 495 longitudinal estuarine circulation as a whole, it can reflect the change in the  
 496 corresponding component for the estuarine circulation (Cheng, 2013). For example, an  
 497 increase or decrease in the baroclinic pressure gradient force can reflect the change in  
 498 the gravitational circulation, and the change in the advection term is representative of  
 499 the change in tidal rectification. In the following, we present the vertically averaged  
 500 values for these different terms along the longitudinal section in different years. It  
 501 should be noted that the friction term consists of a component of the tidally mean eddy

502 viscosity multiplied by the tidally mean vertical current shear, and a component of the  
503 correlation between eddy viscosity and vertical current shear, which is referred to as  
504 the tidal straining (Simpson et al., 1990).

505 Figure 7 shows that during the neap tide, the baroclinic pressure gradient force  
506 was balanced by barotropic gradient force, friction, and advection term in each year.  
507 This is different from the classic estuarine momentum balance (Pritchard, 1956) but  
508 consistent with the recent understanding of estuarine physics (Geyer and MacCready,  
509 2014). The Coriolis force is quite small as both the latitude of the HE and the residual  
510 current are small. The high value of the baroclinic term was observed to shift upstream  
511 over time. As the baroclinic term is the multiplication of the salinity gradient and water  
512 depth, the changes in this term over years can be induced by the change in water depth  
513 and/or the salinity gradient. It can be seen from Fig. 4 that north of the null point, the  
514 salt intrusion gradually moved towards the bayhead with the estuary narrowing, thus  
515 increasing the salinity gradient there. In the meantime, the upstream water depth was  
516 increased due to channel dredging, particularly in 2010. Therefore, the increase of the  
517 baroclinic term was caused by both the increases in water depth and salinity gradient.  
518 Although the barotropic term contributed a lot to the momentum balance, it did not  
519 change obviously with the morphological evolution. The advection term at Sec. B1  
520 increased slightly with the estuary narrowing, especially in the deepening part of the  
521 channel in 2010. The friction term was larger in 2010 than in other years, because the  
522 salt intrusion increased the vertical shear of the longitudinal current at Sec. B1.  
523 Nevertheless, the increase in friction term was much smaller than that of the baroclinic  
524 term. Chant et al. (2018) attributed the increase in exchange flow to the increase in  
525 along-channel salinity gradient and/or a reduction in vertical mixing by deepening, but  
526 in our case, the increase in baroclinic term was dominant and the change in vertical  
527 mixing even posed a reversed effect.





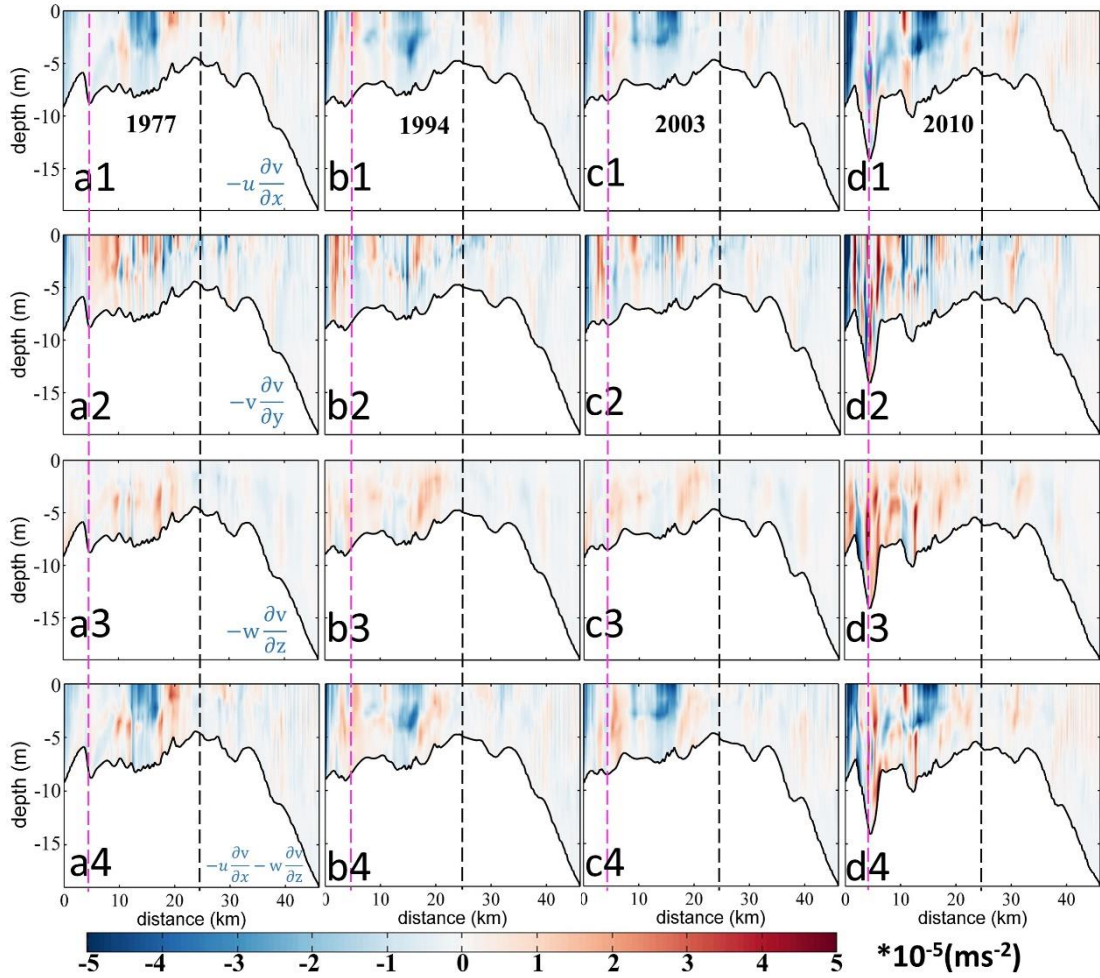
528

529 Fig. 7. Patterns of the tidally-averaged longitudinal momentum terms during neap tide (from  
 530 March 10th 00:00 to 11st 00:00 (25h)) at Sec. A in 1977(a), 1994(b), 2003(c), and 2010(d). The  
 531 starting point of the X-axis is Point A in Fig. 1b. “accel” in legend: local acceleration term (the  
 532 time rate of change of longitudinal flow); “barot” in legend: the barotropic pressure gradient  
 533 force; “baroc” in legend: the baroclinic pressure gradient force.

534

535 To further identify the changes in different terms, the advection term was divided  
 536 into lateral (X-direction), longitudinal (Y-direction), and vertical (Z-direction)  
 537 advection terms (Fig. 8). It is worth noting that the sum of the advection terms in X  
 538 and Z directions represents the effect of the lateral circulation.





539

540 Fig. 8. Patterns of the tidally-averaged longitudinal momentum terms during neap tide (from  
 541 March 10th 00:00 to 11st 00:00 (25h)) at Sec. A. (a1-d1): The advection in the X direction,  
 542  $-u \frac{\partial v}{\partial x}$ . (a2-d2): The advection in the Y direction,  $-v \frac{\partial v}{\partial y}$ . (a3-d3): The advection in the Z  
 543 direction,  $-w \frac{\partial v}{\partial z}$ . (a4-d4): The sum of the advection terms in X and Z directions. 1977, 1994,  
 544 2003, and 2010 cases are in the first, second, third, and fourth columns, respectively. The pink  
 545 and black dotted lines represent the location of Sec.B1 and Sec.B2, respectively. The starting  
 546 point of the X-axis is Point A in Fig. 1b.

547

548 From Fig. 8, in 2010, the advection terms in all directions increased significantly.  
 549 Generally, the lateral and vertical advection competes against each other, and their  
 550 additive effect is to generate a circulation similar to the gravitational circulation. This  
 551 effect was larger in 2010 than in other years (Figs. 8a4-d4). The longitudinal advection  
 552 increased in the upper part of the channel in 2010 (Figs. 8a2-d2), following the

553 deepening and narrowing of the estuary. In the middle of the longitudinal section, the  
 554 tidal residual current shows a seaward flow at the surface and a landward flow at the  
 555 bottom, whereas in the upper portion, it shows a uniform landward flow.

556 Overall, from 1977 to 2010, the baroclinic forcing, the friction, and the advection  
 557 terms increased obviously along the Sec. A. The maximum longitudinal estuarine  
 558 circulation in 2010 was caused by the increase in the pressure gradient force and the  
 559 advection term, especially the baroclinic forcing. The effects of these changes on  
 560 estuarine circulation will be further discussed.

561

#### 562 **4.2 Analysis of the streamwise vorticity balance for the lateral flow**

563

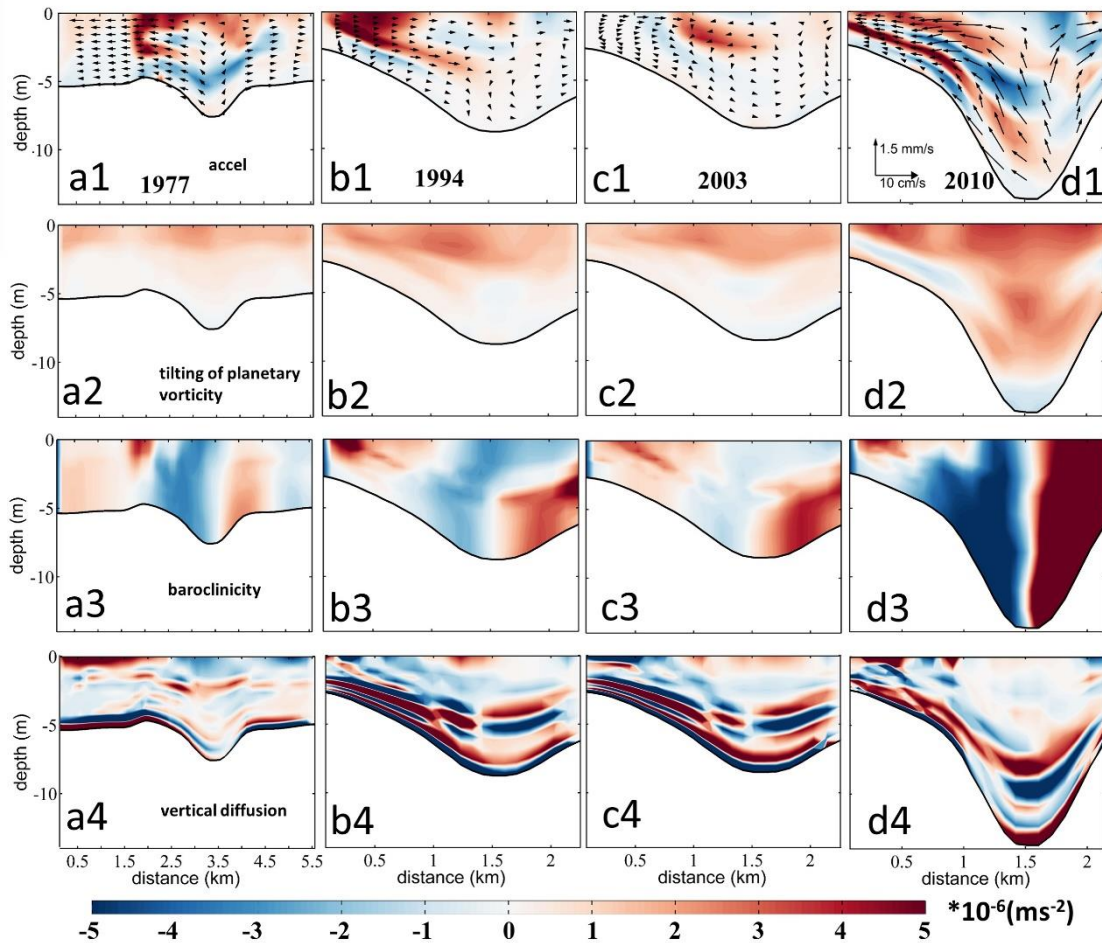
564 In order to reveal the contribution of the vertical shear of the along-channel flow,  
 565 the lateral salinity gradient, and the vertical diffusion to changes in the lateral  
 566 circulation, we examine the changes in terms of the streamwise vorticity transport  
 567 equation (Li et al., 2014):

$$568 \quad \frac{dw_y}{dt} = \underbrace{-f \frac{\partial v}{\partial z}}_{\text{tilting of planetary vorticity}} \underbrace{-g\beta \frac{\partial S}{\partial x}}_{\text{baroclinicity}} \underbrace{+\frac{\partial^2}{\partial z^2}(K_V w_y)}_{\text{vertical diffusion}} \underbrace{+\frac{\partial^2}{\partial x^2}(K_H w_y)}_{\text{horizontal diffusion}}, \quad (5)$$

569 In the right side of Eq. 5, the first term represents the tilting of the planetary  
 570 vorticity by vertical shear in the along-channel flow, the second term is the baroclinicity  
 571 caused by the lateral salinity gradient, the third term is the vertical diffusion, and the  
 572 fourth term is the horizontal diffusion, which is typically two orders of magnitude  
 573 smaller than the vertical diffusion term. Therefore, we only show the acceleration and  
 574 first three right-hand-side terms in Fig. 9.

575 Figure 9 shows that the changes of baroclinic term caused by the water depth  
 576 change dominated the changes in the lateral circulation at Sec. B1. The baroclinic term  
 577 in the deep channel was generally negative at the left side of the channel, and it  
 578 increased significantly in 2010, about 2-3 times the value in 1977. The baroclinic term  
 579 with positive values occurred at the West Shoal over the study period, but the areal  
 580 extent occupied by the positive values decreased gradually, with its magnitude

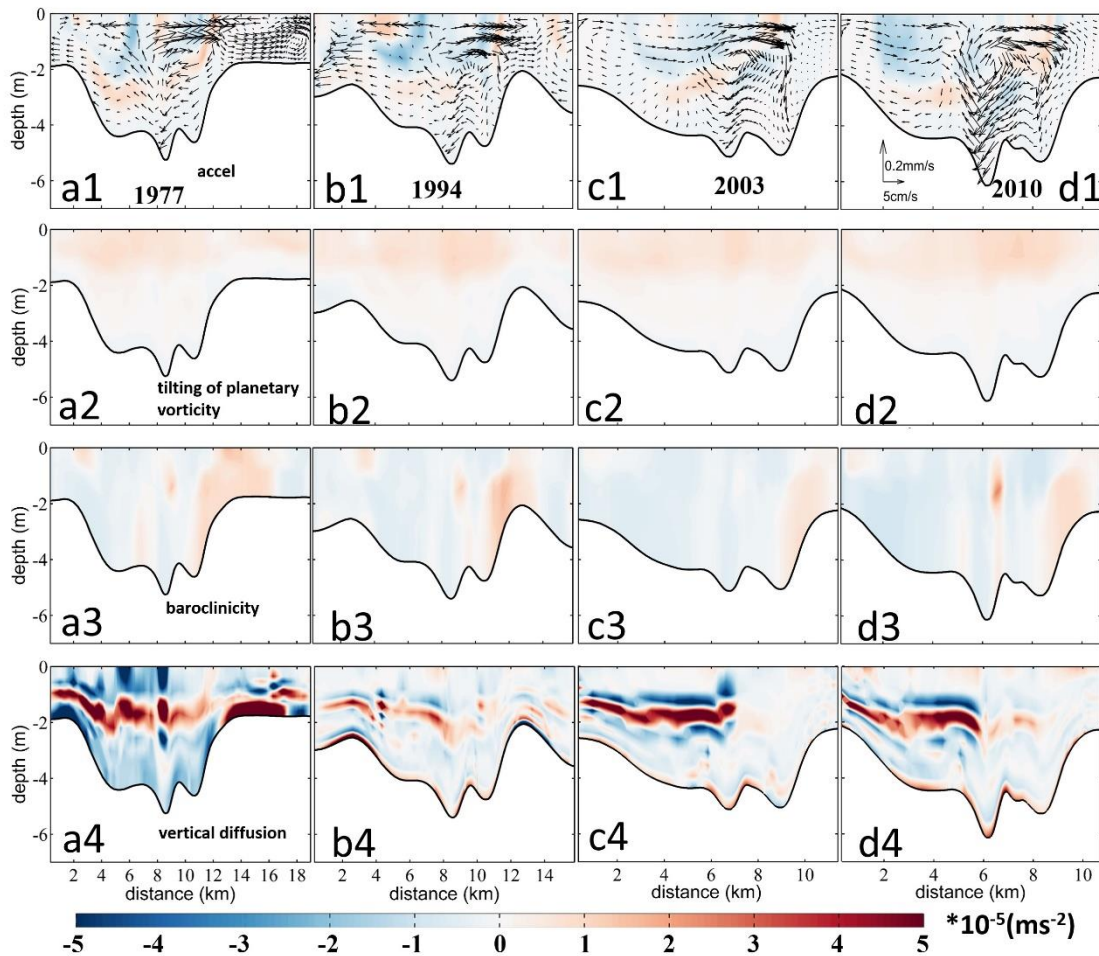
581 increased obviously in 1994 when the narrowing rate was the largest. A negative  
 582 baroclinic term appeared at the bottom of the West Shoal, indicating that the changes  
 583 in water depth can lead to changes in the pattern and magnitude of the baroclinic term,  
 584 which was mainly caused by the changes in the salt intrusion. The tilting of the  
 585 planetary vorticity term increased with the estuary narrowing, with the increase in 2010  
 586 was greater, which was mostly caused by the depth change. The pattern of the vertical  
 587 diffusion term changed significantly in 1977 and 1994, especially at the surface and the  
 588 bottom layers of the West Shoal, indicating that it was the changes in width that altered  
 589 the vertical diffusion term.



590

591 Fig. 9. Patterns of the tidally-averaged streamwise vorticity equation terms during neap tide  
 592 (from March 10th 00:00 to 11st 00:00 (25h)) at Sec. B1. (a1-d1): The local acceleration term  
 593 (the time rate of change of the longitudinal vorticity). (a2-d2): The tilting of planetary vorticity  
 594 term. (a3-d3): The baroclinic term. (a4-d4): The vertical diffusion term. The cases in 1977,  
 595 1994, 2003, and 2010 are in the first, second, third, and fourth columns, respectively. The

596 starting point of the X-axis is Point C in Fig. 2d. For viewing purposes, the acceleration term is  
 597 multiplied by 5. The block arrows in a1-d1 represent the distribution of lateral circulation.  
 598



599  
 600 Fig. 10. Patterns of the tidally-averaged streamwise vorticity equation terms during neap tide  
 601 (from March 10th 00:00 to 11st 00:00 (25h)) at Sec. B2. (a1-d1): The local acceleration term  
 602 (the time rate of change of the longitudinal vorticity). (a2-d2): The tilting of planetary vorticity  
 603 term. (a3-d3): The baroclinic term. (a4-d4): The vertical diffusion term. The cases in 1977,  
 604 1994, 2003, and 2010 are in the first, second, third, and fourth columns, respectively. The  
 605 starting point of the X-axis is Point E in Fig. 2d. For viewing purposes, the acceleration term is  
 606 multiplied by 5. The block arrows in a1-d1 represent the distribution of lateral circulation.  
 607

608 From Fig. 10, the change in the tilting of the planetary vorticity at Sec. B2 was  
 609 analogous to that at Sec. B1. The baroclinic term did not change much, because the  
 610 changes in water depth were smaller in this section. The clockwise circulation over the  
 611 West shoal increased as the estuary deepened in 2010, because the baroclinic term was  
 612 larger with the increase of salt intrusion and vertical salinity gradient near Sec. B2. The

613 vertical diffusion of the vorticity was overall negative, indicating its effect in dissipating  
614 the vorticity. The vertical diffusion term was larger than the baroclinic term, especially  
615 in the middle water, which was inconsistent with the conclusion that the baroclinic term  
616 is the most important one in the lateral circulation (Li et al., 2014). The reason may be  
617 that in our study site, the vertical mixing was strong as the estuary became shallow.  
618 However, the existence of a pycnocline greatly weakened the momentum exchange  
619 between the upper and lower layers: above the pycnocline, the tilting of the planetary  
620 vorticity was dominant; whereas, under the pycnocline, the baroclinic term was  
621 dominant. The decrease of the estuary width changed the magnitude and pattern of the  
622 vertical diffusion term, and the area with a large positive value at the bottom of the East  
623 Shoal disappeared, along with the magnitude of the negative value decreased greatly at  
624 the easternmost of the section. It indicates that in a shallow estuary, the vertical  
625 diffusion term caused by the width change is also important.

626 In Summary, the tilting of the planetary vorticity increased with the decrease of  
627 width or with the increase of water depth. The variation of estuary width was  
628 responsible for the changes in the vertical diffusion term, and the changes in water depth  
629 were responsible for the changes in the baroclinic term. The increase of the longitudinal  
630 estuary circulation can increase the baroclinic term at the cross-sections by increasing  
631 the salinity gradient near the cross-sections, which mainly occurred in the periods of  
632 the estuary deepening. The deepening rate of Sec.B1 was the highest (61%) in 2010,  
633 which led to the strongest lateral circulation in 2010. The lateral circulation intensity  
634 decreased when the estuary narrowed in 2003 due to the decreased baroclinic term. In  
635 addition, the shallowing was the main reason for the pattern change of the lateral  
636 circulation at Sec.B2. At Sec. B2, the narrowing rate was the largest in 2003, and the  
637 adjustment of the vertical diffusion term resulted in an increased lateral circulation from  
638 1994 to 2003. The decrease of the clockwise circulation at the East Shoal was mainly  
639 related to the adjustment of the vertical diffusion term to the baroclinic term.  
640

641 **4.3 Comparison to theoretical results and other estuaries influenced by human**  
642 **interventions**

643

644 The longitudinal estuarine circulation is generated by the river discharge, Stokes  
645 return flow, longitudinal baroclinic pressure gradient force, tidal straining, and  
646 advection (Geyer and Maccready, 2014). The HE features a microtidal tidal regime  
647 (tidal range less than 1.5 m), and the component generated by the baroclinic pressure  
648 gradient, i.e., the gravitational circulation, would be a primary part of the longitudinal  
649 estuarine circulation. The convergent geometry makes it susceptible to the residual flow  
650 induced by the longitudinal advection (Burchard et al., 2014). However, as seen above,  
651 the horizontal advection (especially the longitudinal advection term) also plays a role  
652 in generating the estuarine circulation.

653 With channel deepening and width narrowing in the HE, the gravitational  
654 circulation was increased by the increased baroclinic pressure gradient force. Based on  
655 Geyer's research (2010), the gravitational circulation can be simplified to:

656 
$$v_g = a_1(\beta g s_0 R w_0 h_0)^{1/5} U_0^{2/5} w^{-2/5} h^{-1/5}, \quad (6)$$

657 in which  $w_0$  and  $h_0$  is the width and depth at the estuary mouth, respectively. It  
658 indicates that the gravitational circulation is inversely related to the water depth and  
659 width in the estuary, with a weaker dependence on the water depth. In Chant et al.  
660 (2018), the gravitational circulation is completely unrelated to the water depth in their

661 equation (2), which is  $v_g \propto \left(\frac{g'R}{w}\right)^{\frac{1}{3}}$ , in which the  $g'$  is the reduced gravity acceleration.

662 This seems to contradict the situations occurring in many estuaries, such as in the Coos  
663 Bay (Eidam et al., 2020), Tampa Bay (Zhu et al., 2015), Changjiang Estuary (Zhu,  
664 2018), Ems estuary (Van Maren et al., 2015), Hudson Estuary (Ralston and Geyer,  
665 2019), and Newark Bay of the Delaware estuary (Chant et al., 2018). In all these  
666 estuaries, the gravitational circulation demonstrated an increase with the deepening of  
667 the channel. It suggests that the changes in gravitational circulation vary in different

668 parts of the estuary and the longitudinal salinity gradient may not catch up with the  
669 change in water depth in the analytical solution, as proposed by Chant et al. (2018) and  
670 Ralston and Geyer (2019). In our study site, the salinity gradient at the upstream part  
671 of the longitudinal section was increased owing to an enhanced salt intrusion where  
672 water depth increased, which led to an increased gravitational circulation in the upper  
673 HE (Fig. 4).

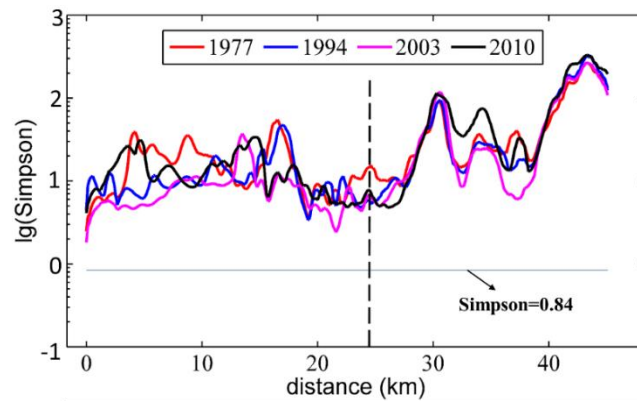
674 The tidal straining-induced estuarine circulation is another important component of  
675 longitudinal estuarine circulation. The straining-induced circulation is the covariance  
676 of the eddy viscosity and the vertical shear of the longitudinal flow (ESCO) in a tidal  
677 cycle and is included in the term of internal friction. Cheng et al. (2010) have indicated  
678 that ESCO-induced flow dominates the gravitational circulation in periodically  
679 stratified estuaries with strong tides, having the same structure as the gravitational  
680 circulation. It has the same order of magnitude in weakly stratified estuaries with  
681 moderate tides, and is less important in highly stratified estuaries with weak tides, even  
682 with a reversed structure with the gravitational circulation. As indicated by Becherer et  
683 al. (2015), the strength of the straining-induced circulation is dependent on the Simpson  
684 number (or the horizontal Richardson number). The Simpson number is expressed as:

685 
$$S_i = g\beta \frac{ds}{dy} \frac{h^2}{u_*}, \quad (7)$$

686 in which  $u_*$  is the bottom friction velocity, represented by  $u_* = \sqrt{C_d}U_t$ , where  $C_d$  is  
687 the bottom friction coefficient and  $U_t$  is the tidal velocity amplitude.

688 When  $S_i$  is larger than 0.84, the water column is in a persistent stratified situation,  
689 and the straining-induced circulation becomes weaker. We calculated the  $S_i$  along the  
690 longitudinal section in different years and depict them in Fig. 11.





691

692 Fig. 11. Distribution of the Simpson number in different years along the longitudinal section.  
 693 The Y-axis represents the logarithm of the  $S_i$ . The black dotted line represents the location of  
 694 the null point.

695 It indicates that along the longitudinal section, the  $S_i$  number was mostly above  
 696 the criterion of 0.84, showing that the straining-induced circulation is not significant.  
 697 The  $S_i$  number was the smallest in 2003 and the largest in 2010. It indicates that with  
 698 the narrowing and deepening of the HE, the straining-induced circulation became  
 699 weaker. This is consistent with Burchard et al. (2014) and Schulz et al. (2015). It  
 700 indicates that with the human interventions, the straining-induced circulation became  
 701 less important in the longitudinal estuarine circulation.

702 For the advection-induced longitudinal estuarine circulation, we noted that the  
 703 longitudinal and vertical advection terms were smaller than the lateral advection. Based  
 704 on Cheng and Valle-Levinson (2009), the lateral advection-induced longitudinal  
 705 circulation is proportional to the ratio of  $h/(wK_m)$ , where  $w$  is the width, and  $K_m$  is  
 706 the eddy viscosity. It shows that in a narrower and deeper estuary, the lateral advection  
 707 has a larger effect in influencing the longitudinal estuarine circulation. Lerczak and  
 708 Geyer (2004) also showed that the effect of the lateral advection on longitudinal  
 709 circulation is stronger for narrower estuaries. Our results show that with the narrowing  
 710 and deepening of the estuary, not only the lateral advection but also the longitudinal  
 711 advection has great influences on the longitudinal estuarine circulation.

712



713 **4.4 The possible future development of the estuarine circulation and its**  
714 **implications**

715

716 The pattern of lateral circulation during the dry season in the HE experienced a  
717 dramatic change from 2003 to 2010 in the West Shoal at Sec. B2, from an under-  
718 developed circulation structure to a complete clockwise vortex in 2010. This transition  
719 was associated with the increase in lateral salinity gradient, the increase in longitudinal  
720 bottom landward flow, and a decrease of friction by the increased water depth and  
721 stratification.

722 The mechanisms for the lateral circulation during the wet season have been  
723 revealed by Chen et al. (2020b), who showed that it was primarily driven by the  
724 barotropic process, i.e., the water elevation gradient, and thus by the intensity of the  
725 ebb jet. Different from the wet season when the river discharge was higher, the lateral  
726 circulation in the dry season was more affected by the baroclinic effect. We speculate  
727 that, with the narrowing and deepening of the estuary, the lateral circulation will be  
728 enhanced even in the wet season accompanied by the strengthened ebb jet in the deep  
729 channel.

730 In the HE, the channel underwent siltation, and sediment was carried from the  
731 channels to side banks by the lateral circulation, making the estuary overall shallower  
732 in 2003. In 2005, dredging of the channel increased the channel depth (Luo, 2010), and  
733 increased the longitudinal estuarine circulation, though the lateral circulation decreased  
734 slightly by the smaller rate of convergence. If reclamation did not occur as frequently  
735 as it did in the last century, and the channel dredging continued, the circulation of HE  
736 will keep increasing as the water depth increasing, and thus a positive feedback exists.  
737 However, as revealed in Eq. (6) and Eq. (2) in Chant et al. (2018), with the increase in  
738 salt intrusion, the longitudinal salinity gradient will decrease, showing negative  
739 feedback. Moreover, Schulz et al. (2015) noted that estuarine circulation exhibited a  
740 distinct maximum in medium-wide channels by comparing estuarine circulation under  
741 different width-to-depth ratios. In our study, as shown in Table 4, the width-to-depth

742 ratio has been decreasing from 1977 to 2010, but the estuarine circulation has been  
743 increasing. The difference would be caused by the fact that in our study site, the tidal  
744 mixing is not strong enough to generate an effective tidal straining-induced circulation.

745 The changes in the estuarine circulation have important implications for sediment  
746 transport and morphological evolution in the HE. With the increase of longitudinal  
747 estuarine circulation, the sediment trapping effect is expected to be enhanced, thus more  
748 riverine sediment would be trapped inside the estuary. In the meantime, the change in  
749 lateral circulation would decrease the sediment advection from the channel to the West  
750 Shoal, which occurred in the wet season and was favorable for the siltation in the West  
751 Shoal (Chen et al., 2020b).

752 Being a micro-tidal partially mixed estuary with standing tidal wave, the estuarine  
753 circulation in HE is stronger during the neap tide than during the spring tide. After  
754 analyzing the circulation during spring tide, we found the longitudinal circulation  
755 reached maximum in 2010 when the water depth was the largest. Similar to the  
756 phenomenon during the neap tide, the longitudinal circulation was dominated by the  
757 increase in the baroclinicity. However, the changes in the lateral circulation were more  
758 complicated than that during the neap tide. In addition to the baroclinicity, the change  
759 in vertical diffusion caused by the width change also played an important role. The  
760 changes in lateral circulation at the upstream section (Sec. B1) were mostly controlled  
761 by the changes in the baroclinicity. On the other hand, the changes in lateral circulation  
762 at the downstream section (Sect. B2) were mainly controlled by the changes in the  
763 vertical diffusion.

764 In this study, the model used was only driven by river discharge and tides, without  
765 considering the effects of winds, waves, sea level rise, and other upstream flows into  
766 the estuary. Future work could incorporate the above factors to improve the model's  
767 accuracy. Sea level rise can increase the total water depth and inundate more intertidal  
768 areas. It has an effect similar to that of channel deepening, to increase the salt intrusion  
769 and estuarine circulation. The river flow will be generally decreased in the PRD due to  
770 global warming and northward shift of the climate zone. With a decrease of the river

771 discharge, the salt intrusion will be increased and thus the salinity gradient will be  
772 decreased, resulting in a weakened estuarine circulation in the HE. For the salinity at  
773 the offshore boundary, we are not certain whether it will be increased or decreased. It  
774 is influenced by the rain and evaporation, and the large-scale salt transport in the South  
775 China Sea. If it increases, the salinity gradient in the HE will be increased, and the  
776 estuarine circulation will be enhanced therefore. And vice versa.

777         Definitely, the estuary has undergone natural changes in 40+ years, such as the  
778 changes in river inflow, offshore boundary conditions. But as we mentioned, our focus  
779 is on the impact of changes in bathymetry on the estuarine circulation, and the paper  
780 has already been much lengthy, we leave the effect of other factors for future  
781 investigation. It should be noted that our model simulations are not used to reproduce  
782 exactly the historical evolution, but to reveal the underlying dynamics.

783

## 784 **5. Conclusion**

785

786         This study investigated the morphological evolution of the HE from 1977 to 2010  
787 using ArcGIS and remote sensing. It was noted that the West Channel of the HE  
788 disappeared, causing the morphological pattern to change from “two channels and  
789 three shoals” gradually to “one channel and two shoals” throughout the years. Due to  
790 the reclamation and development of salt marshes along the estuarine banks, the estuary  
791 has been experiencing continuous narrowing. Meanwhile, channel dredging has  
792 deepened the estuary over the study period. It had been revealed that the sediment  
793 transport pattern changes in response to the changes in river discharge and tidal mixing  
794 (Gong et al., 2014). Generally, there exists a sediment convergence zone in the middle  
795 of the estuary, and the riverine sediment is trapped inside the estuary to form a  
796 turbidity maximum. Our results indicate that the intensity of the longitudinal estuarine  
797 circulation kept increasing as the estuary width continued to decrease. The trend of the

798 lateral circulation intensity altered (decreased at Sec. B1 and increased at Sec. B2)  
799 when the estuary shallowed (from 1994 to 2003).

800 The changes in the longitudinal estuarine circulation were dominated by the  
801 changes in the baroclinic pressure gradient force and advection. As the estuary was  
802 narrowing and deepening, the pressure gradient force and advection term (especially  
803 the longitudinal advection term) increased, which increased the longitudinal  
804 circulation. The change in lateral circulation intensity was mainly caused by the  
805 change of the vertical shear of the longitudinal subtidal flow, the lateral salinity  
806 gradient, and the vertical dissipation term. The changes in water depth were the  
807 dominant factor affecting lateral circulation intensity. The increase of water depth  
808 enhanced the longitudinal circulation and the lateral circulation of the upstream cross-  
809 section in 2010. The changes in the estuarine circulation have great implications for  
810 the sediment transport in the HE, which would be explored in the next step.

811

#### 812 **Data availability**

813 A total of 142G data of 66 images (Table 1) covering the PRD during cloudless days  
814 in multiple years (from 1973 to 2018) were downloaded from <http://www.gscloud.cn/>.

815

#### 816 **Author contributions**

817 RuiZhang: Writing - original draft, model runs and analyses. Bo Hong: Writing -  
818 review. Lei Zhu: Writing - review. Wenping Gong: Writing - review & editing,  
819 Conceptualization, Funding acquisition. Heng Zhang: Visualization, Funding  
820 acquisition.

821

#### 822 **Competing interests**

823 The authors declare that they have no conflict of interest.

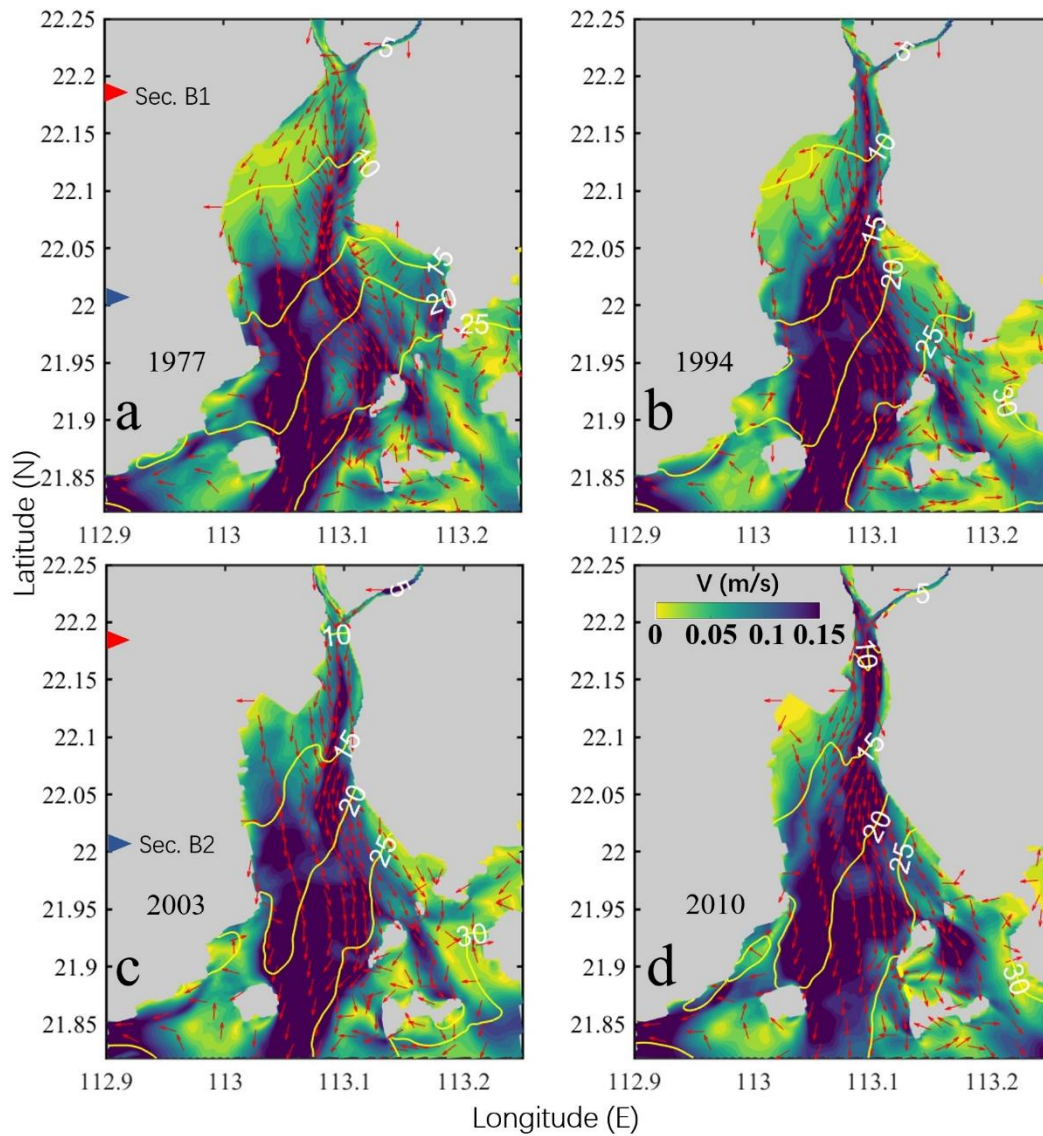
824

#### 825 **Acknowledgments**

826 This research is funded by the National Natural Science Foundation of China [Grant  
 827 nos. 51761135021, 41506102, 41890851]. We would like to thank the National  
 828 Aeronautics and Space Administration (NASA) for providing the Landsat remote  
 829 sensing data. We are very grateful to graduate students in our team from Sun Yat-sen  
 830 for their help in fieldwork and sediment sample analysis in the indoor laboratory.

831

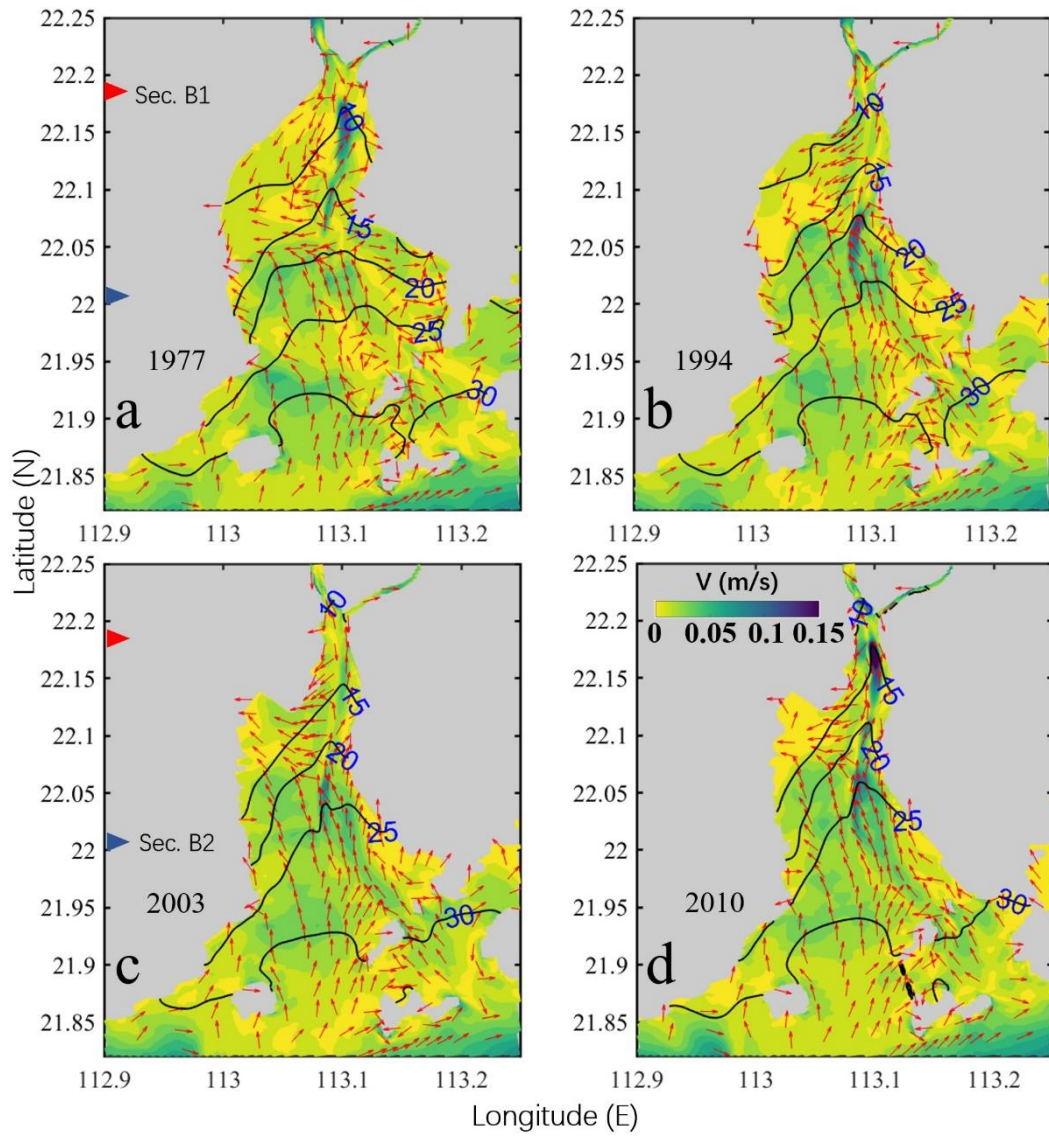
832 **Appendix A**



833

834 Fig. A. 1. Patterns of the tidally and vertically averaged horizontal circulation at the surface  
 835 during neap tide (from March 10th 00:00 to 11st 00:00 (25h)) in 1977(a1), 1994(a2), 2003(a3),  
 836 and 2004(a4). The magnitude of the current is represented by the color shading, while the

837 current direction is shown by the arrows. The salinity is depicted by the contour lines. The red  
 838 and blue triangles depict the positions of two cross-sections (Sec.B1 and Sec.B2).  
 839



840  
 841 Fig. A. 2. Patterns of the tidally and vertically averaged horizontal circulation at the bottom  
 842 during neap tide (from March 10th 00:00 to 11st 00:00 (25h)) in 1977(a1), 1994(a2), 2003(a3),  
 843 and 2004(a4). The magnitude of the current is represented by the color shading, while the  
 844 current direction is shown by the arrows. The salinity is depicted by the contour lines. The red  
 845 and blue triangles denote the positions of two cross-sections (Sec.B1 and Sec.B2).  
 846

847 **References**

848  
 849 Ai, B., Zhang, R., Zhang, H., Ma, C. L. and Gu, F. G.: Dynamic process and artificial mechanism of  
 850 coastline change in the Pearl River Estuary, *Regional Studies in Marine Science*, 30, 100715, 2019.  
 851 Amin, M.: On perturbations of harmonic constants in the Thames Estuary, *Geophysical Journal of the*

852 Royal Astronomical Society, 73, 587-603, 1983.

853 Becherer, J., Stacey, M. T., Umlauf, L. and Burchard, H.: Lateral circulation generates flood tide  
854 stratification and estuarine exchange flow in a curved tidal inlet, *J. Phys. Oceanogr.*, 45, 638-656,  
855 2015.

856 Burchard, H., Hetland, R. D., Schulz, E. and Schuttelaars, H. M.: Drivers of Residual Estuarine  
857 Circulation in Tidally Energetic Estuaries: Straight and Irrotational Channels with Parabolic Cross  
858 Section, *J. Phys. Oceanogr.*, 41, 548-570, 2010.

859 Burchard, H., Schulz, E. and Schuttelaars, H. M.: Impact of estuarine convergence on residual circulation  
860 in tidally energetic estuaries and inlets, *Geophys. Res. Lett.*, 41, 913-919, 2014.

861 Chant, R. J., Sommerfield, C. K. and Talke, S. A.: Impact of channel deepening on tidal and gravitational  
862 circulation in a highly engineered estuarine basin, *Estuar. Coast.*, 41, 1587-1600, 2018.

863 Chen, L. H., Gong, W. P., Scully, M. E., Zhang, H., Cheng, W. C. and Li, W.: Axial wind effects on  
864 stratification and longitudinal sediment transport in a convergent estuary during wet season, *Journal*  
865 *of Geophysical Research: Oceans*, 125, e2019J-e15254J, 2020a.

866 Chen, L. H., Gong, W. P., Zhang, H., Zhu, L. and Cheng, W. C.: Lateral circulation and associated  
867 sediment transport in a convergent estuary, *Journal of Geophysical Research: Oceans*, 125, e2019J-  
868 e15926J, 2020b.

869 Chen, S. N., Geyer, W. R., Ralston, D. K. and Lerczak, J. A.: Estuarine Exchange Flow Quantified with  
870 Isohaline Coordinates: Contrasting Long and Short Estuaries, *J.phys.oceanogr*, 42, 748-763, 2012.

871 Chen, S. N. and Sanford, L. P.: Axial Wind Effects on Stratification and Longitudinal Salt Transport in  
872 an Idealized, Partially Mixed Estuary, *J. Phys. Oceanogr.*, 39, 1905-1920, 10.1175/2009JPO4016.1,  
873 2009.

874 Cheng, P.: Decomposition of Residual Circulation in Estuaries, *Journal of Atmospheric & Oceanic*  
875 *Technology*, 31, 698-713, 2013.

876 Cheng, P. and Valle-Levinson, A.: Influence of lateral advection on residual currents in microtidal  
877 estuaries, *J. Phys. Oceanogr.*, 39, 3177-3190, 2009.

878 Cheng, P., Valle-Levinson, A. and De Swart, H. E.: Residual currents induced by asymmetric tidal  
879 mixing in weakly stratified narrow estuaries, *J. Phys. Oceanogr.*, 40, 2135-2147, 2010.

880 Chernetsky, A. S., Schuttelaars, H. M. and Talke, S. A.: The Effect of Tidal Asymmetry and Temporal  
881 Settling Lag on Sediment Trapping in Tidal Estuaries, *Ocean Dynam.*, 60, 1219-1241, 2010.

882 Dyer, K. R. 1977. Lateral circulation effects in estuaries. *National Academy of Sciences*, p. 22-29.

883 Eidam, E. F., Sutherland, D. A., Ralston, D. K., Dye, B., Conroy, T., Schmitt, J., Ruggiero, P. and Wood,  
884 J.: Impacts of 150 Years of Shoreline and Bathymetric Change in the Coos Estuary, Oregon, USA,  
885 *Estuar. Coast.*, 1-19, 2020.

886 Fischer, H. B.: Mixing and Dispersion in Estuaries, *Annu. Rev. Fluid Mech.*, 8, 107-133,  
887 10.1146/annurev.fl.08.010176.000543, 1976.

888 Geyer, W. R.: Estuarine salinity structure and circulation, *Contemporary issues in estuarine physics*, 12,  
889 26, 2010.

890 Geyer, W. R. and Maccready, P.: The Estuarine Circulation, *Annu. Rev. Fluid Mech.*, 46, 175-197, 2014.

891 Geyer, W. R. and Nepf, H.: Tidal pumping of salt in a moderately stratified estuary, *Coastal and estuarine*  
892 *studies*, 213-226, 1996.

893 Gong, W. P., Jia, L. W., Shen, J. and Liu, J. T.: Sediment transport in response to changes in river  
894 discharge and tidal mixing in a funnel-shaped micro-tidal estuary, *Cont. Shelf Res.*, 76, 89-107,

895 2014.

896 Gong, W. P., Liu, H., Ren, J. and Yu, H. B.: The study of tidal propagation in the Huangmaohai estuary  
897 and its underlying mechanisms, *Acta Oceanol. Sin.*, 34, 41-54, 2012.

898 Gong, W. P., Schuttelaars, H. and Zhang, H.: Tidal asymmetry in a funnel-shaped estuary with mixed  
899 semidiurnal tides, *Ocean Dynam.*, 66, 637-658, 2016.

900 Huang, T. 2011. Study on abnormal changes of tidal range in the huangmaohai estuary. Guangdong  
901 Water Resources and Hydropower, Guangzhou, China.

902 Jia, L. W., Luo, J. and Ren, J.: The analysis of the evolution of a sand bar and its formation in the  
903 Huangmao Bay in the Pearl River Delta, *Acta Oceanol. Sin.*, 34, 120-127, 2012.

904 Kjerfve, B., Stevenson, L. H., Proehl, J. A., Chrzanowski, T. H. and Kitchens, W. M.: Estimation of  
905 material fluxes in an estuarine cross section: A critical analysis of spatial measurement density and  
906 errors 1, *Limnol. Oceanogr.*, 26, 325-335, 1981.

907 Lacy, J. R., Stacey, M. T., Burau, J. R. and Monismith, S. G.: Interaction of lateral baroclinic forcing and  
908 turbulence in an estuary, *Journal of Geophysical Research: Oceans*, 108, 1-34,  
909 <https://doi.org/10.1029/2002JC001392>, 2003.

910 Lerczak, J. A. and Rockwell Geyer, W.: Modeling the Lateral Circulation in Straight, Stratified  
911 Estuaries\*, *J. Phys. Oceanogr.*, 34, 1410-1428, 2004.

912 Lesser, G. R., Roelvink, J. V., Van Kester, J. and Stelling, G. S.: Development and validation of a three-  
913 dimensional morphological model, *Coast. Eng.*, 51, 883-915, 2004.

914 Li, C. Y. and O'Donnell, J.: Tidally driven residual circulation in shallow estuaries with lateral depth  
915 variation, *Journal of Geophysical Research Oceans*, 102, 27915-27929, 1997.

916 Li, M., Cheng, P., Chant, R. J., Valle-Levinson, A. and Arnott, K.: Analysis of vortex dynamics of lateral  
917 circulation in a straight tidal estuary, *J. Phys. Oceanogr.*, 44, 2779-2795, 2014.

918 Li, W., Shi, J. Z., Pu, X. and Hu, G. D.: Circulation within curved channel of the north passage in the  
919 changjiang river estuary: a vorticity approach, *Oceanologia et Limnologia Sinica*, 48, 682-694, 2017.

920 Li, Y. B. 2019. Numerical simulation of the formation and evolution of the geomorphic characteristics  
921 of Huangmao Sea. Dalian University of Technology, Dalian, China.

922 Luo, J. 2010. Cause Analysis of Morphological evolution of Huangmao sea Estuary in the Decade to  
923 Century-scale. Sun Yat-sen university, Guangzhou, China.

924 Pritchard, D. W.: Salinity distribution and circulation in the Chesapeake Bay estuarine system.. 1, *Mar.*  
925 *Res*, 11, 106-123, 1952.

926 Pritchard, D. W.: The dynamic structure of a coastal plain estuary, *J Marine Res*, 15, 33-42, 1956.

927 Ralston, D. K. and Geyer, W. R.: Response to channel deepening of the salinity intrusion, estuarine  
928 circulation, and stratification in an urbanized estuary, *Journal of Geophysical Research: Oceans*,  
929 124, 4784-4802, 2019.

930 Salles, P., Valle-Levinson, A., Sottolichio, A. and Senechal, N.: Wind - driven modifications to the  
931 residual circulation in an ebb - tidal delta: Arcachon Lagoon, Southwestern France, *Journal of*  
932 *Geophysical Research Oceans*, 120, 728-740, 2015.

933 Schulz, E., Schuttelaars, H. M., Gr We, U. and Burchard, H.: Impact of the depth-to-width ratio of  
934 periodically stratified tidal channels on the estuarine circulation, *J. Phys. Oceanogr.*, 45, 411804097,  
935 2015.

936 Scully, M. E., Geyer, W. R. and Lerczak, J. A.: The Influence of Lateral Advection on the Residual  
937 Estuarine Circulation: A Numerical Modeling Study of the Hudson River Estuary, *J. Phys.*



938 Oceanogr., 39, 107-124, 10.1175/2008JPO3952.1, 2009.

939 Scully, M. E., Geyer, W. R. and Lerczak, J. A.: The Influence of Lateral Advection on the Residual  
940 Estuarine Circulation: A Numerical Modeling Study of the Hudson River Estuary, *J. Phys.*  
941 *Oceanogr.*, 39, 107-124, 10.1175/2008JPO3952.1, 2009.

942 Scully, M., Friedrichs, C. and Brubaker, J.: Control of estuarine stratification and mixing by wind-  
943 induced straining of the estuarine density field, *Estuaries*, 28, 321-326, 10.1007/BF02693915, 2005.

944 Simpson, J. H., Brown, J., Matthews, J. and Allen, G.: Tidal straining, density currents, and stirring in  
945 the control of estuarine stratification, *Estuaries*, 13, 125-132, 10.2307/1351581, 1990.

946 Van Maren, D. S., van Kessel, T., Cronin, K. and Sittoni, L.: The impact of channel deepening and  
947 dredging on estuarine sediment concentration, *Cont. Shelf Res.*, 95, 1-14, 2015.

948 Wang, T., Geyer, W. R., Engel, P., Jiang, W. S. and Feng, S. Z.: Mechanisms of Tidal Oscillatory Salt  
949 Transport in a Partially Stratified Estuary, *J. Phys. Oceanogr.*, 45, 2773-2789, 2015.

950 Waterhouse, A., Tutak, B., Valle-Levinson, A. and Sheng, Y.: Influence of Two Tropical Storms on the  
951 Residual Flow in a Subtropical Tidal Inlet, *Estuar. Coast.*, 36, 1037-1053, 10.1007/s12237-013-  
952 9606-3, 2013.

953 Willmott, C. J.: On the validation of models, *Phys. Geogr.*, 2, 184-194, 1981.

954 Wilson, R. and Filadelfo, R. 1986. Subtidal Current Variability in the Lower Hudson Estuary. Springer -  
955 Verlag, Berlin, Germany. p. 132-142.

956 Winterwerp, J. C.: Fine sediment transport by tidal asymmetry in the high-concentrated Ems River:  
957 indications for a regime shift in response to channel deepening, *Ocean Dynam.*, 61, 203-215, 2011.

958 Zhang, R., Chen, L. H., Liu, S. S., Zhang, H. and Lin, G. Y.: Shoreline evolution in an embayed beach  
959 adjacent to tidal inlet: The impact of anthropogenic activities, *Geomorphology*, 346, 106856, 2019.

960 Zhu, J., Weisberg, R. H., Zheng, L. Y. and Han, S. Z.: Influences of Channel Deepening and Widening  
961 on the Tidal and Nontidal Circulations of Tampa Bay, *Estuaries & Coasts*, 38, 132-150, 2015.

962 Zhu, L. 2018. Alteration of estuarine circulation under the inference of morphological evolution. East  
963 China Normal University, Shanghai, China.

964